Lack of cortistatin exacerbates neuroimmune and vascular dysfunction in ischemic stroke

Castillo-González J[1,2,3*], Vargas-Rodríguez P[1], Serrano-Martínez I[1], Cuenca-Martagón A[1], Forte-Lago I[1], Price M[2,3], Buscemi L[2,3], Hirt L[2,3], Ruiz JL[1,4], González-Rey E[1*].

[1]Institute of Parasitology and Biomedicine (IPBLN-CSIC), Granada, Spain; [2]University of Lausanne, Lausanne, Switzerland; [3]Lausanne University Hospital, Lausanne, Switzerland; [4]Functional Genomics Center Zurich, ETH Zurich and University of Zurich, Zurich, Switzerland

*Correspondence: elena.g@csic.es; Julia.CastilloGonzalez@unil.ch; Tel.: +34-958-181670

Summary

Ischemic stroke remains a leading cause of mortality and disability worldwide, with few therapies addressing its complex pathophysiology. Neuroinflammation, blood–brain barrier disruption, and immune dysregulation contribute to acute damage and long-term decline. Cortistatin, an immunomodulatory neuropeptide, has shown therapeutic benefit in acute stroke, though its endogenous role during onset and recovery remains unknown. Using an integrative approach combining transcriptomics from human and murine datasets, a preclinical stroke model, and tissue-level analysis in young and middle-aged mice, we demonstrated the causal and protective role of cortistatin during acute and subacute stroke phases. Our findings reveal that cortistatin deficiency increases stroke susceptibility and worsens outcomes. The lack of cortistatin triggers an amplified transcriptional response to ischemia, driving heightened neuroinflammation, glial dysfunction, compromising neurovascular integrity, and suppressing repair-associated pathways. Indeed, cortistatin levels were inversely associated with stroke severity. Notably, cortistatin deficiency accelerated aging-associated pathological features following stroke, underscoring its relevance in neuroimmune and cerebrovascular health. Administration of exogenous cortistatin reversed many detrimental effects, improving neuronal survival, mitigating immune dysregulation, preserving myelin, and promoting vascular recovery. Overall, cortistatin emerges as a key endogenous regulator of stroke

26 pathophysiology and a promising multimodal therapy, supporting neuroimmune integrative
27 approaches to tackle the multifaceted nature of stroke.

28 **INTRODUCTION**

29 Ischemic stroke is the second leading cause of mortality worldwide and the main contributor
30 of adult disability [1]. The interruption of cerebral blood flow initiates a cascade of
31 interconnected events, including neuroinflammation, blood-brain barrier (BBB) disruption, and
32 immune deregulation, major hallmarks of stroke pathogenesis [2]. Despite advancements of
33 recanalization therapies, current treatments remain limited to intravenous recombinant tissue
34 plasminogen activator (rtPA) and endovascular thrombectomy, both with narrow therapeutic
35 window and considerable adverse effects [3]. Therapeutic shortcomings arise from simplistic
36 preclinical models that overlook key risk factors like aging, the administration of single-target
37 drugs in a multifactorial disorder, and overemphasis on immunosuppressive rather than
38 immunomodulatory therapies. Additionally, poor understanding of the complex spatiotemporal
39 pathophysiology of stroke affecting simultaneously the brain, vasculature, and often-
40 overlooked peripheral organs, presents additional challenges [4]. Consequently, deeper
41 comprehension of the neuroimmune context and the roles of endogenous mediators across
42 acute and subacute stages of ischemic pathology is essential for developing more effective
43 therapeutic strategies.

44 Cortistatin, a neuropeptide distributed throughout the central nervous system (CNS)
45 and the immune system [5,6], may play a prominent role in this context. Despite sharing
46 homology, functions, and receptors (SSTR1-5) with somatostatin, cortistatin performs distinct
47 roles in the nervous system and peripheral tissues [7,8], interacting also with the ghrelin
48 receptor (GHSR), Mas gene-related receptor X-2, and an unidentified cortistatin-specific
49 receptor. Remarkably, cortistatin exhibits potent immunomodulatory, anti-inflammatory, and
50 neuroprotective effects in models of neuroinflammatory/neuroimmune disorders, including
51 multiple sclerosis [9], excitotoxicity [10], meningoencephalitis [11], neuropathic pain [12], and
52 Parkinson's disease [13]. In these models, cortistatin reduces pro-inflammatory mediators,

53 modulates glial function, and preserves tissue-surveillance, protecting against disease onset
54 and progression. Cortistatin also affects BBB integrity by regulating tight-junction (TJ) proteins
55 and exerting anti-inflammatory actions on endothelial cells, protecting against ischemic
56 damage and barrier leakage [14]. A recent study from our group highlighted its therapeutic
57 benefits when administered 24h post-stroke in young mice [15]. However, its impact on stroke-
58 associated risk factors and its long-term beneficial effects remains unknown. Additionally,
59 cortistatin endogenous role in stroke pathophysiology is not fully understood. Previous
60 research from our group demonstrated that its deficiency causes higher baseline peripheral
61 inflammation and lower production of neurotrophic factors [6,9]. Cortistatin-deficient mice also
62 exhibited worsened outcomes in models of local inflammation and neuronal injury [9,12,16].

63 Given the important benefits of cortistatin in neuroprotection, immunomodulation, and
64 BBB preservation, we aim to further investigate its endogenous and therapeutic functions in
65 preclinical stroke. Our study examines for the first time the role of cortistatin in stroke pathology
66 across young and middle-aged deficient mice, focusing on acute and subacute outcomes. Our
67 findings position cortistatin as both a central regulator of neurovascular and immune
68 responses in stroke, and a multimodal therapeutic candidate. Unlike most current interventions
69 that target isolated downstream events or require narrow timing, cortistatin appears to operate
70 across multiple stages of stroke pathology, broadening the therapeutic window and suggesting
71 new strategies for intervention that go beyond clot retrieval and reperfusion.

72

73 **MATERIALS AND METHODS**

74 ***Peptides***

75 Lyophilized mouse cortistatin (CST-29) was obtained from Bachem and dissolved in distilled
76 water to a final concentration of 10^{-4} M.

77 ***Animals***

78 The experimental protocols employed in this study were approved by the Animal Care and
79 Use Board and the Ethical Committee of the Spanish National Research Council (Animal Care
80 Unit Committee IPBLN-CSIC # protocol CEEA OCT/2017.EGR) and conducted in accordance
81 with Directive 2010/63/EU of the European Parliament on the protection of animals used for
82 scientific purposes. Transgenic mice deficient in the cortistatin gene (*Cort*$^{-/-}$), generously
83 provided by Dr Luis de Lecea (Stanford University, United States), were bred and maintained
84 on a C57BL/6J background as previously described [7]. Mice were housed in groups of ten
85 per cage under controlled environmental conditions (22 ± 1ºC, 60-70% relative humidity) with
86 a 12h light/dark cycle (lights on at 7:00 a.m.), with *ad libitum* access to food and water.

87 ***Transient middle cerebral artery occlusion model***

88 Young (12 weeks old) and middle-aged (6 months old) *Cort*$^{+/+}$ and *Cort*$^{-/-}$ male mice were
89 subjected to the MCAO model as previously described [17]. Anaesthesia was induced using
90 isoflurane (1.5-2% in 70% N_2O/30% O_2) via a facemask, and meloxicam (2mg/kg, Norbrook)
91 was administered subcutaneously for post-surgery analgesia. Body temperature was
92 maintained constant throughout the procedure using a heating pad. Regional cerebral blood
93 flow (rCBF) was continuously monitored by laser Doppler flowmetry (moorVMS-LDF1, Moor
94 Instruments) fixing a probe on the skull over the core area supplied by the middle cerebral
95 artery (MCA) (approximately 1 mm posterior and 6 mm lateral to the bregma). Transient focal
96 ischemia was induced by introducing a silicon-coated filament (701756PK5Re, Doccol)
97 through the left common carotid artery into the internal carotid artery to occlude the MCA. The
98 occlusion was maintained for 20 min in young mice and 35 min in middle-aged mice, after
99 which the filament was withdrawn to allow reperfusion. This combination of occlusion time and
100 filament size resulted in a mild MCAO model [15]. The surgery was considered successful if
101 the rCBF decreased below 20% of the baseline during occlusion and recovered above 50%
102 of the baseline upon reperfusion. Following surgery, mice were returned to their cages with
103 *ad libitum* access to food and water. Each cage was supplied with water-softened chow and
104 recovery gel.

105 Cortistatin (144 µg/kg) was administered intraperitoneally 24h after MCAO, either as a
106 single dose (endpoint at 48h) or daily for 7 days. Control groups received equivalent volumes
107 of saline solution. Neurological assessments, behavioural tests, ischemic volume
108 determination, morphometric characterization of glial population, and inflammatory response
109 evaluation were determined at 48h (acute) and 7 days after surgery (subacute).

110 ***Neurological and behavioural assessments***

111 The functional outcome of each mouse was evaluated using a neurological score every 24h
112 following MCAO and prior to sacrifice. Neurological severity was graded on a scale from 0 to
113 3, assessing motor, sensory, reflex, and balance functions, based on a combination of
114 established scoring systems [18,19].

115 In addition, muscle coordination and endurance were analysed using the wire-hanging
116 test. Mice were suspended on a custom-made apparatus consisting of a single wire stretched
117 between two posts over a soft surface. Training was conducted 24h before surgery, and
118 performance was evaluated at 48h and 5 days post-MCAO, recording the number of
119 successful reaches (defined as the mouse touching either the right or left post) or falls [20].
120 The test concluded after 180s or when a mouse fell from the wire ten times. Motor skills were
121 further characterized using the pole test, which measured the ability of mice to grip and
122 descend a vertical pole to a safe surface [21]. Mice underwent one training trial 24h before
123 surgery. Post-surgical evaluations of mice were conducted 48h and 5 days after MCAO.
124 Performance was scored based on successful descents or falls (reaching the mat or falling
125 onto it, respectively). The total time taken to reach the mat with at least two limbs, along with
126 the number of turns required to descend, were recorded. The test concluded after three trials,
127 if any trial exceeded 120s, or after three falls.

128 ***Ischemic lesion volume determination***

129 At 48h or 7 days post-MCAO, mice were sacrificed by an overdose of intraperitoneal ketamine
130 (100 mg/kg, Ritcher Pharma) and xylazine (10 mg/kg, Fatro Iberica), followed by intracardial

131 perfusion with 4% PFA. Brains were dissected, post-fixed in 4% PFA for 24h at 4ºC, and then
132 cryoprotected in 30% sucrose for 48h at 4ºC. Subsequently, brains were frozen in isopentane
133 on dry ice at –25ºC and stored at –80ºC until further processing. Coronal brain sections were
134 cut at a thickness of 20 µm using a cryostat.

135 Serial sections were stained with cresyl violet (CV) following a protocol of gradual
136 hydration in ethanol, staining with 1 mg/ml of CV-acetate in distilled water, gradual dehydration
137 in ethanol, and clearing in xylene [19]. Stained sections were imaged using a Leica DM2000
138 Transmit stereomicroscope at 2.5x magnification, and infarcted areas were measure using the
139 ImageJ Fiji free software. Infarct volume was calculated by summing the infarcted areas from
140 each section and multiplying by the spacing distance between sections.

141 ***Immunofluorescence***

142 Free-floating brain sections (20 µm-thick) were first washed with PBS, then blocked and
143 permeabilized using a solution of PBS 1x, 1% bovine serum albumin (BSA), 0.1% Triton X-
144 100, and 5% goat serum for 60 min at RT. The sections were subsequently incubated
145 overnight at 4ºC with primary antibodies anti-MAP2 (1:1,000, Sigma), anti-Iba1 (1:1,000,
146 Wako), anti-GFAP (1:5,000, Dako), anti-CD31/PECAM-1 (1:300, BD), anti-ZO-1 (1:100,
147 Fisher), anti-VEGF (1:500, Abcam) or APC-labelled anti-CD45 (1:200, BD) diluted in PBS 1x
148 with 1% BSA, 0.1% Triton X-100, and 5% goat-serum. Next, sections were washed with PBS
149 and then incubated with the appropriate Alexa Fluor-conjugated secondary antibodies
150 (1:1,000, Sigma) and DAPI in PBS 1x, 1% BSA, 0.1% Triton X-100, and 2% goat-serum for
151 60 min. Sections were mounted using Mowiol. For IgG staining, the same protocol was
152 followed, except that an Alexa Fluor 594-conjugated goat anti-mouse IgG antibody was used
153 without a primary antibody. Images were obtained with a LEICA DMi8 S Platform Life-cell
154 microscope at 20x magnification and a Leica TCS SP8 STED confocal microscope at 63x
155 magnification.

156 ***Morphometric analyses of microglial phenotypes***

157 To thoroughly characterize the complex and heterogeneous morphology of
158 microglia/infiltrating macrophages following stroke, we performed extensive morphometric
159 analyses. First, individual microglia/macrophages from specific brain regions, such as the
160 periinfarct area, were randomly selected. Attention was warranted to avoid cell overlap and to
161 ensure complete capture of both the soma nucleus and cellular branches. A total of 15-30
162 cells per mouse from 3-6 mice (N=3-6) were analysed. Image processing was performed using
163 ImageJ Fiji software, following a systematic protocol adapted from previous studies [13,22,23].
164 Initially, images were converted to 8-bit grayscale and pre-processed to reduce background
165 noise and enhance contrast. Subsequently, images were binarized using a pre-determined
166 threshold, and non-cellular artefacts were removed using the *remove outliers* and *despeckle*
167 functions. In cases where significant background noise was present, manual editing was
168 performed to refine the segmentation.

169 After image processing, morphometric parameters were obtained using the *skeleton* and
170 *fractal analysis* plugins in ImageJ Fiji [24]. For *skeleton analysis*, the number of junctions and
171 maximum branch length were quantified. For *fractal analysis*, key parameters included the
172 convex hull area (the minimal convex polygon enclosing the entire cell structure), span ratio
173 (defined as the ratio of the major to minor axes of the convex hull), and fractal dimension (an
174 index representing cellular complexity).

175 ***Determination of the peripheral immune response***

176 To characterize the peripheral immune activity, we evaluated the levels of immune mediators
177 and the spleen response. To quantify peripheral inflammatory factors, blood samples were
178 collected by cardiac puncture, allowed to clot for 2h at RT, and then centrifuged at 2,000rpm
179 for 10 min. The serum concentration of the factors was measured using a sandwich ELISA
180 assay. Maxisorb plates (Millipore) were coated overnight at 4ºC with capture antibodies (anti-
181 IL-6 and anti-IL-12 from BD Pharmigen, or anti-MCP-1 from PeproTech). Plates were washed
182 with PBS containing 0.05% Tween-20 and then blocked with PBS containing 10% fetal bovine
183 serum (FBS) for 2h. Serum samples and recombinant standards were added to the plates and

184 incubated overnight at 4°C. After incubation, biotinylated detection antibodies (Serotec) were
185 applied for 1h at RT. Following washing, plates were incubated with avidin-HRP (Sigma)
186 (1:500 in blocking buffer) for 1h and developed using ABTS substrate (Sigma). Absorbance
187 was measured at 405nm with a spectrophotometer (Molecular Devices), and the
188 concentrations of inflammatory factors were calculated based on the standard curve
189 generated concurrently.

190 Spleens were collected, weighed, and gently dissociated into a 100 mm culture dish.
191 The homogenized tissue was transferred into RPMI medium supplemented with 10% FBS, 2
192 mM L-glutamine, 1% P/S, and 50 μM 2-mercaptoethanol. The suspension was then let to sit
193 on ice for 5 min, and the cell suspension was carefully collected and centrifuged at 1,670 rpm
194 for 10 min at 4°C. The resulting pellet was resuspended in Ack lysis buffer (150 mM NH_4Cl,
195 10 mM $KHCO_3$, 0.1 mM Na_2EDTA) for 10 min at RT to lyse red blood cells. RPMI medium was
196 added, and the cells were centrifuged again at 1,670 rpm for 10 min at RT before being
197 counted.

198 ***RNA extraction and evaluation of gene expression***

199 After MCAO, brains were collected at the specified time points (*i.e.,* 48h and 7 days) and
200 separated into contralateral and ipsilateral hemispheres. For RNA isolation, brain tissue was
201 placed in TriPure reagent (Roche). cDNA synthesis from 20 ng RNA per sample was
202 performed using the RevertAid First Strand cDNA Synthesis Kit (ThermoFisher) with random
203 hexamers in a CFX Connect QPCR System (Biorad) under the following conditions: incubation
204 at 25°C for 5 min, reverse transcription at 42°C for 60 min, inactivation at 70°C for 5 min. Gene
205 expression analysis was performed using conventional qPCR. cDNA was added to the
206 SensiFast Sybr No-Rox kit 1x (Bioscience), along with forward and reverse primers specific to
207 each gene and nuclease-free water to reach a final volume of 20 μl. The qPCR reactions were
208 run in a CFX96 thermocycler (BioRad) under the following conditions: initial polymerase
209 activation at 94°C for 5 min, 40 cycles at 94°C for 30s (denaturation), 58°C/60°C/62°C for 30s
210 (primer-specific annealing), and 72°C for 30s (extension). Gene expression quantification was

211 performed using the comparative threshold cycle (Ct) method, with Ct values normalized to
212 those of the housekeeping gene *Rplp0*. Fold change was calculated using the ΔΔCt method.
213 The specific primers for each gene are listed in Additional File 1: Table S1.

214 ***Next-generation transcriptome sequencing (RNA-seq) and data analysis***

215 RNA (200 ng) from contralateral (CL, healthy) and ischemic (MCAO) brain hemispheres
216 isolated from *Cort*$^{+/+}$ and *Cort*$^{-/-}$ mice 48h post-stroke was used to prepare mRNA libraries with
217 the Illumina stranded mRNA Prep Ligation kit (Illumina, San Diego, CA, USA). Three (CL) and
218 five (MCAO) independent biological replicates were used with RNA Integrity Number
219 coefficients >8.7 (Bioanalyzer RNA 6000 Nano-chip, Agilent). Quality and size distribution of
220 mRNA libraries were validated using the Bioanalyzer High Sensitivity DNA assay, and their
221 concentrations were measured on a Qubit fluorometer (ThermoFisher). Final libraries were
222 pooled in equimolecular ratios and converted to single-stranded circular DNA with MGIEasy
223 Universal Library Conversion kit (MGI Tech, Shenzhen) for sequencing on MGI platforms. The
224 100 bp paired-end sequencing was conducted on a DNBSEQ-G400 sequencer (MGI Tech,
225 Shenzhen). The average percentage of sequencing reads above a quality score of Q>30 was
226 96.3%, with a mean GC content of 50.0%, and over 44 million reads per sample.

227 We implemented the reanalyzerGSE v3.0.0 software [25] in the RNA-seq analysis to
228 identify differentially expressed genes (DEGs) and to prevent the exclusion of lowly expressed
229 genes with potential biological relevance, such as cortistatin (see details in Additional File 2).
230 We detected >45,000 transcripts. Multidimensional scaling (Principal Coordinates Analysis,
231 PCoA) and unsupervised hierarchical clustering of normalized samples were performed to
232 assess the divergence and the replicability of samples from each independent comparison.
233 DEGs with a False Discovery Rate (FDR) <0.05 were calculated by comparing: i) *Cort*$^{-/-}$ *vs.*
234 *Cort*$^{+/+}$ samples for each condition (CL and MCAO); ii) MCAO *vs.* CL for each genotype (*Cort*$^{-}$
235 $^{/-}$ and *Cort*$^{+/+}$). The log2 fold change ($\log_2$FC) was used to quantify gene expression changes.
236 To explore the functional significance of DEGs, we performed two different approaches: an

237 over-representation analysis based on the Gene Ontology (GO) database [26,27] and a Gene
238 Set Enrichment Analysis (GSEA), as indicated in Additional File 2.

239 ***Cell-specific gene sets and cell type proportion estimation***

240 Cell-type–specific gene sets were obtained from both the default settings of the
241 markerGeneProfile R package v1.0.4 [28] and the curated marker sets reported by Zheng et
242 al [29]. Both sources include overlapping gene markers for microglia, astrocytes, and
243 oligodendrocytes; however, the astrocyte and oligodendrocyte gene sets differ in composition
244 and biological meaning between the two approaches. Unlike other marker databases that rely
245 on a single data source, these marker sets represent a consensus from several published
246 studies and account for brain regional heterogeneity. We use both gene sets to estimate
247 marker gene profiles (MGPs), which serve as a proxy for relative changes in cell type
248 proportions. For this, we used as input the transcript-per-million (TPM) normalized gene
249 expression data from our RNA-seq. Details on how MGPs were derived can be found in
250 Additional File 2. Additionally, both gene sets were used to assess the enrichment of our
251 samples for the specified cell markers by performing a GSEA as a complementary analysis.

252 ***Integration of human and mouse datasets for cortistatin gene expression analysis***

253 Cortistatin gene expression levels were obtained from the Gene Expression Omnibus
254 database (GEO), incorporating datasets from human and mouse samples following stroke.
255 For humans, we analysed data from: peripheral blood mononuclear cells (PBMCs) from
256 ischemic patients at acute and subacute stroke stages (GSE122709) [30]; and with/without
257 haemorrhagic transformation (GSE199435) [31]; leukocytes from patients with differential
258 stroke severity (GSE202709) [32]; and brain tissue dissected from healthy controls and acute
259 ischemic stroke patients post-mortem (GSE56267) [33]. Mouse data from cortical tissue were
260 obtained from different experimental stroke models, such as MCAO model (GSE253799,
261 unpublished; GSE227186 [34]); cerebral venous sinus thrombosis (CVST) model
262 (GSE245455, unpublished); and photothrombotic (PT) stroke model (GSE261613,

263 GSE184917 [35,36]; GSE280846, unpublished). Details of these datasets can be found in
264 Additional File 2.

265 ***Statistical analysis***

266 Data are expressed as the mean ± SEM. All experiments were randomized and conducted in
267 a blinded manner. The number of independent animals (N), as well as the number of sections,
268 cells, or structures analysed (n), are indicated for each experiment. Comparisons between two
269 groups were analysed using the unpaired Student's t test for parametric data with normal
270 distribution or the Mann-Whitney U-test for non-parametric data. For comparisons involving
271 three or more groups with normally distributed parametric data, one-way ANOVA with Fisher´s
272 LSD *post-hoc* test was employed. For non-parametric data involving three or more groups,
273 the Kruskal-Wallis test with a Dunn *post-hoc* test was used. When standard deviations were
274 assumed to be different, Brown-Forsythe and Welch ANOVA tests were applied, followed by
275 a Dunnett T3 *post-hoc* test. All analyses were performed using GraphPad Prism v8.3.0
276 software. For the statistical approaches used in the sequencing data analyses, see the section
277 above. We considered p-values <0.05 as significant.

278 ***Data availability***

279 RNA-seq data are available in the GEO repository under accession number GSE302342,
280 https://www.ncbi.nlm.nih.gov/geo/query/acc.cgi?acc=GSE302342. Reviewers may access
281 the record while private with the token ilwxqkgwxzyfjmd.

282 **RESULTS**

283 ***Cortistatin is downregulated in ischemic stroke***

284 To investigate the potential involvement of cortistatin in ischemic stroke, we first assessed its
285 expression levels in both human and murine models of cerebral ischemia. Due to the limited
286 availability of post-mortem human brain tissue and murine blood samples, we primarily used
287 peripheral blood mononuclear cells from patients (PBMCs and leukocytes) and mouse brain
288 tissue. Our results show that cortistatin expression was markedly reduced in PBMCs in acute

289 and subacute stroke phases and was inversely associated with stroke severity (Fig. 1a). Post-
290 mortem human brain samples confirmed decreased cortistatin after ischemia (Fig. 1a).
291 Similarly, mouse brain tissue exhibited significant cortistatin downregulation across multiple
292 stroke paradigms, including transient MCAO, CVST, and PT (Fig.1b). Notably, our transient
293 MCAO model also resulted in cortistatin downregulation, which was partially reversed by
294 exogenous addition of the neuropeptide (Fig. 1c). These findings implicate cortistatin
295 downregulation as a consistent feature of ischemic stroke pathology.

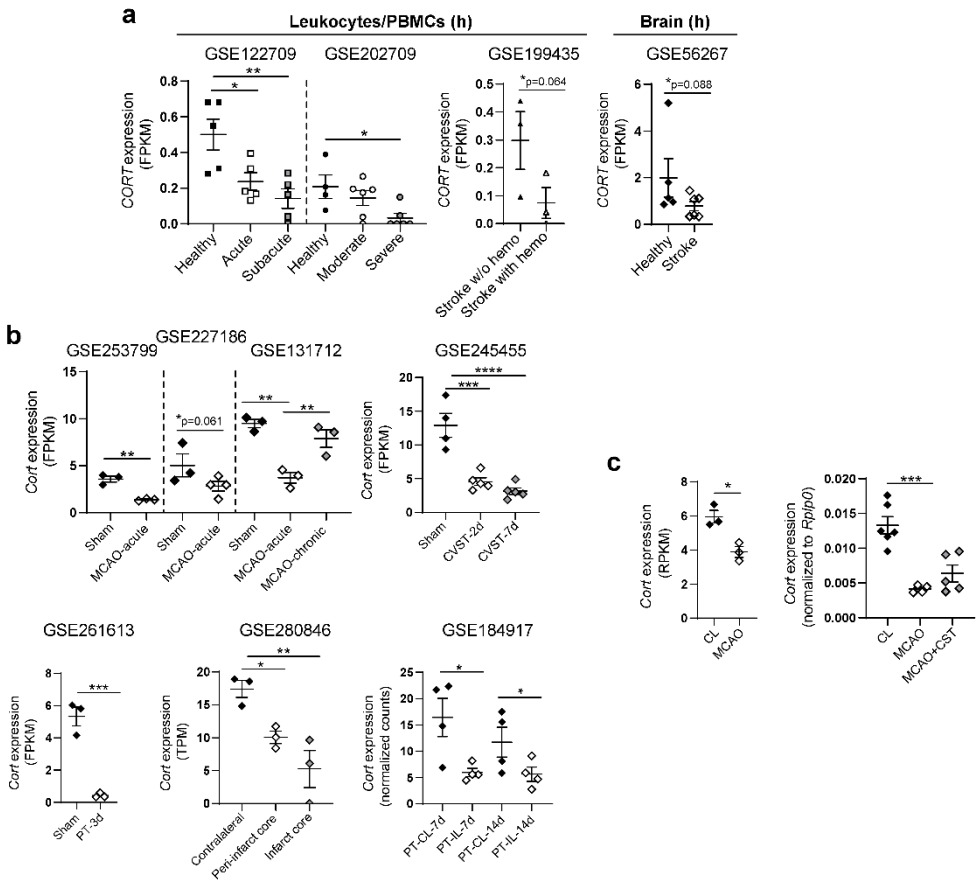

296

297 **Figure 1. Cortistatin gene expression is downregulated following ischemic stroke in both human**
298 **and mouse.** Cortistatin gene expression levels (normalized RPKM, FPKM, TPM, or count values) were
299 obtained from the Gene Expression Omnibus (GEO) database. **a**. Left, expression of cortistatin in
300 human PBMCs from healthy individuals (N=5) and ischemic stroke patients at acute (24h, N=5) and
301 subacute (7 days, N=5) stages (GSE122709); in peripheral leukocytes from patients with moderate
302 (NIHSS score <8, N=6) and severe (NIHSS score ≥8, N=6) ischemic stroke, compared to healthy
303 controls (N=4) (GSE202709); and in PBMCs from ischemic stroke patients with large artery occlusion
304 undergoing thrombectomy, with or without subsequent intracranial haemorrhage (N=3 each)
305 (GSE199435). Right, cortistatin expression in cortical brain tissue of deceased ischemic stroke patients,
306 using matched contralateral healthy tissue as control (N=5 each group). **b**. Top left, cortistatin
307 expression in cortex from sham and ischemic mice subjected to 60 min MCAO and sacrificed at 24h
308 (GSE253799: peri-infarct cortex and GSE227186: peri-lesion, N=3 each), and in ipsilateral cortex from
309 sham and MCAO mice (60 min) sacrificed at 24h (acute phase) or 28 days after stroke (chronic phase)

310 (GSE131712, N=3 each). Top right, cortistatin expression in the cortex of sham (N=4) and mice that
311 underwent cerebral venous sinus thrombosis (CVST), analysed at 2- and 7-days post-injury (N=5 each)
312 (GSE245455). Bottom, cortistatin expression in photothrombotic (PT) models: left, sham and peri-infarct
313 cortex 3 days post-injury (GSE261613, N=3 each); centre, contralateral, peri-infarct and infarct core
314 regions 7 days post-injury (GSE280846, N=3 each); right, contralateral and peri-infarct cortex at 7- and
315 14-days post-stroke (GSE184917, N=4 each). **c**. Left, cortistatin expression in contralateral/ipsilateral
316 hemispheres of MCAO mice (20 min, sacrificed at 48h), analysed by RNA-seq in this study. Right,
317 qPCR validation normalized to *Rplp0*. Data are expressed as mean ± SEM with dots representing
318 individual mice. *$p \leq 0.05$, **$p \leq 0.01$, ***$p \leq 0.001$, ****$p \leq 0.0001$. CL: contralateral; CST: cortistatin; FPKM:
319 fragments per kilobase of transcript per million mapped reads; IL: ipsilateral; MCAO: transient middle
320 cerebral artery occlusion; NIHSS: National Institute of Health Stroke Scale; RPKM*:* reads per kilobase
321 of exon per million reads mapped; TPM*:* transcripts per million.

322 ***Deficiency in cortistatin enhances immune activity, vascular disorganization, and***
323 ***neurodegenerative responses following ischemic stroke***

324 Given that lower cortistatin gene expression was associated with more severe strokes, we
325 investigated whether cortistatin deficiency plays a role in stroke pathophysiology by analysing
326 the transcriptomic profiles of both cortistatin-deficient (*Cort*$^{-/-}$) and wild-type mice (*Cort*$^{+/+}$)
327 subjected to mild MCAO, a model that recapitulates key features of human ischemic condition
328 [37].

329 Comparative analysis revealed minimal baseline transcriptomic differences in non-
330 ischemic hemispheres, with 25 DEGs (15 upregulated, 10 downregulated in *Cort*$^{-/-}$ mice;
331 FDR<0.05) (Table S2; Fig. S1a). Similarly, ischemic hemispheres displayed 27 DEGs
332 between genotypes (12 upregulated, 15 downregulated in *Cort*$^{-/-}$ mice), most of which were
333 common across ischemic and healthy brain (Table S3; Fig. S1a,b). However, GSEA of
334 cortistatin-deficient ischemic brain samples revealed significant upregulation of innate
335 immunity, antiviral defence, pattern recognition receptor signalling, pro-inflammatory cytokine
336 responses (IFN-γ, IL-6, and TNF), and extracellular matrix (ECM) remodelling (Table S4; Fig.
337 S1c).

338 To identify cortistatin-specific responses to ischemia, we compared transcriptomic data
339 from contralateral to ischemic hemispheres within each genotype. *Cort*$^{+/+}$ mice exhibited 443
340 DEGs (419 upregulated and 24 downregulated in the injured tissue), whereas *Cort*$^{-/-}$ mice
341 showed a markedly heightened response with 1483 DEGs (1213 upregulated and 270
342 downregulated) (Fig. 2a; Tables S5, S6). Although substantial DEG overlap was observed
343 between genotypes (Fig. 2b), *Cort*$^{-/-}$ mice demonstrated a more robust enrichment across

344 biological processes (BP) terms including innate and adaptive immune activation, leukocyte
345 infiltration, inflammation, cell cycle progression, ERK1/ERK2, JAK-STAT and MAPK
346 signalling, neuroinflammation, gliogenesis, ECM remodelling, angiogenesis, and ROS
347 metabolism (Fig. 2c; Table S7). Additional enrichment was observed in cellular components
348 (CC) related to membrane specialization, ECM structure; mitotic spindle formation, and
349 adhesion-related protein complexes (Table S8; Fig. S2); as well as in molecular functions (MF)
350 such as immune receptor activity, integrin and molecular factor binding, cytoskeletal
351 remodelling, and GTPase and kinase activity (Table S9; Fig. S3).

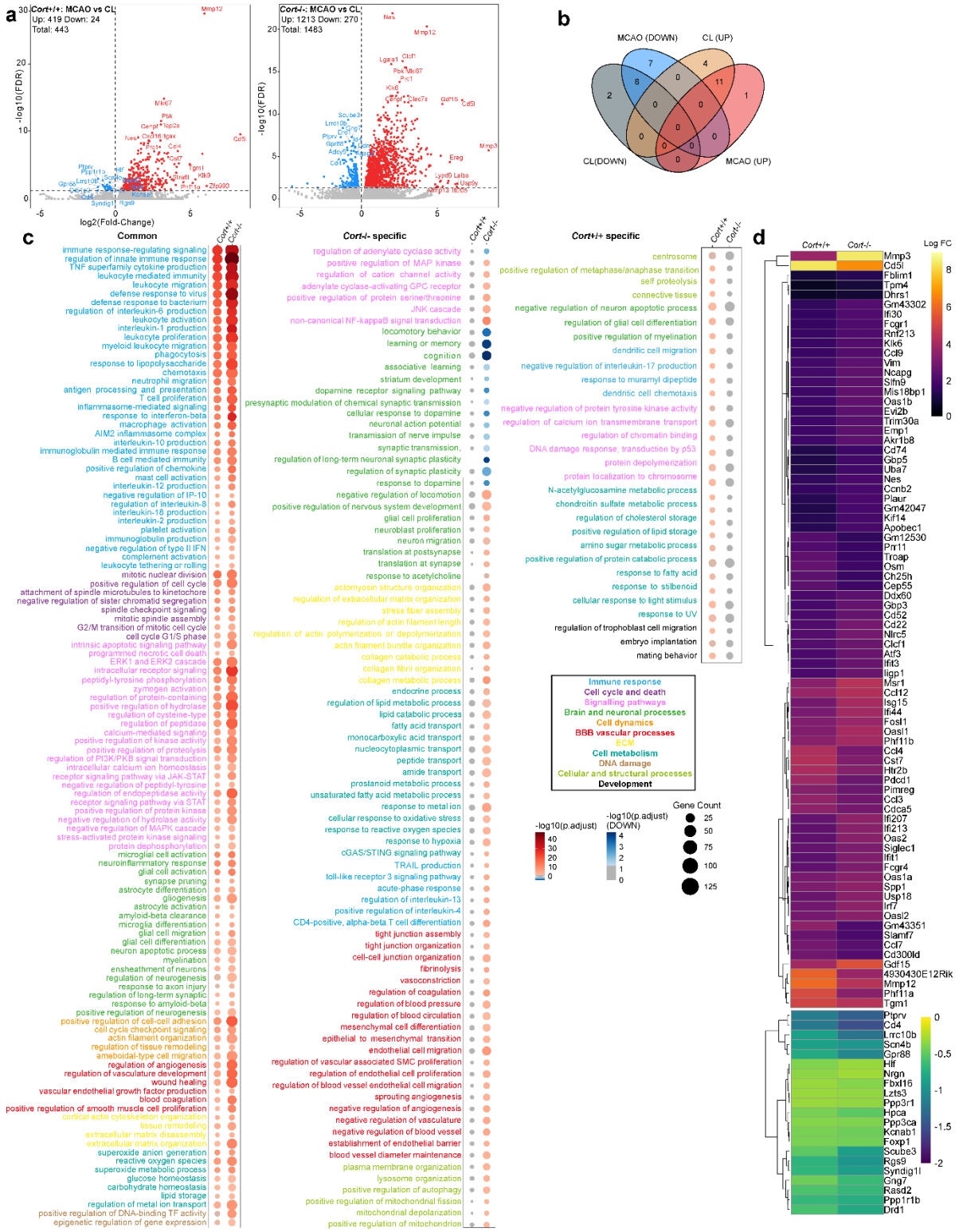

352

353 **Figure 2. Lack of cortistatin leads to an exaggerated transcriptional response to cerebral**
354 **ischemia.** Transcriptomic profiling was performed on *Cort*$^{-/-}$ and *Cort*$^{+/+}$ mouse brains 48h after ischemic
355 stroke induction (20 min MCAO). **a.** Volcano plots depict differentially expressed genes (DEGs) in
356 ischemic (MCAO) *vs.* healthy contralateral (CL) hemispheres from *Cort*$^{+/+}$ (left) and *Cort*$^{-/-}$ (right) mice.
357 Each dot represents one gene. Grey dots represent non-significantly altered genes. Significantly
358 upregulated (red) and downregulated (blue) genes (with false discovery rate, FDR <0.05) during
359 ischemic injury are shown. Comprehensive DEG lists are available in Additional file 1: Tables S5 and
360 S6. **b.** Venn diagram displays the overlap of significantly upregulated and downregulated genes in *Cort*$^{-}$

361 $^{-/-}$ and *Cort*$^{+/+}$ mice. **c.** Gene ontology (GO) enrichment analysis of biological processes revealed distinct
362 and shared terms between healthy and ischemic brain in *Cort*$^{-/-}$ compared to *Cort*$^{+/+}$. DEGs were
363 manually categorized into functional networks including: immune response (blue), cell cycle and death
364 (purple), signalling pathways (pink), brain and neuronal processes (green), cell dynamics (orange), BBB
365 and vascular processes (red), extracellular matrix (ECM, yellow), cell metabolism (turquoise), DNA
366 damage (brown), cellular and structural processes (pistachio green), and development (black). Shared
367 and genotype-specific terms are indicated. All GO terms and corresponding genes are listed in
368 Additional file 1: Table S7. Colour intensity represents statistical significance (red: upregulated, blue:
369 downregulated, grey: non-significant). Circle size reflects the number of DEGs in each pathway. **d.**
370 Heatmap of Log_2FC values for common DEGs across both genotypes. Hierarchical clustering is shown
371 for shared upregulated (top, selected 78/407 genes) and downregulated (bottom, 21/21 genes)
372 transcripts. Full description of DEGs provided in Additional file 1: Table S10.
373

374 Beyond shared responses to ischemia, cortistatin-deficient mice exhibited distinct
375 upregulation of BP involving JNK and non-canonical NF-kappaB signalling, glial proliferation,
376 ECM organization, lipid and amide metabolism, BBB regulation, and mitochondrial integrity.
377 Unique enrichment in CC and MF categories included endosomal/lysosomal compartments,
378 MHC complexes, cell division, cytoskeletal components, Golgi and ribosomal membranes
379 (CC); and inhibitor and protein kinase activities, transcriptional regulation, molecular binding,
380 and transporter function (MF). In contrast, terms exclusively enriched in *Cort*$^{+/+}$ animals
381 primarily involved regulation of glial differentiation, myelination, lipid/cholesterol storage, and
382 mating behaviour (BP); cell cycle and Ser/Thr complexes (CC); oxidoreductase activity,
383 hyaluronic and ferric iron binding (MF). Strikingly, only *Cort*$^{-/-}$ mice demonstrated significant
384 downregulation of gene sets associated with cognition, motor behaviour, dopaminergic
385 signalling, synaptic plasticity (BP); neuronal spine, synapses, and postsynaptic structures
386 (CC); and channel, neurotransmitter and glutamate receptor activities (MF) (Fig. 2c; Tables
387 S7-9; Fig. S2,3).

388 Analysis of 428 DEGs shared between genotypes (407 upregulated, 21 downregulated
389 in ischemia; Table S10), revealed genotype-specific expression changes when comparing
390 stroke-induced Log_2FC differences between genotypes (Log_2FC *Cort*$^{+/+}$ (MCAO *vs.* CL) –
391 Log_2FC *Cort*$^{-/-}$ (MCAO *vs*. CL)) (Fig. 2d). Genes with greater upregulation in *Cort*$^{-/-}$ animals
392 were associated with immune activation, persistent neuroinflammation, gliosis, BBB
393 breakdown, ECM and vascular remodelling, oxidative stress, and impaired neuroprotection
394 (Table S11). Additionally, several genes with undefined roles in stroke but highly upregulated

395 in *Cort*$^{-/-}$ mice may contribute to glial priming and post-ischemic inflammation. Conversely,
396 *Cort*$^{+/+}$ mice showed enhanced upregulation of genes involved in inflammation resolution,
397 tissue repair, and neurogenesis (Table S12). Genes more strongly downregulated in *Cort*$^{-/-}$
398 mice, though their roles in stroke are not fully established, have been implicated in
399 neuroinflammation, vascular instability, impaired synaptic plasticity, disrupted GPCR, and
400 dopamine signalling in other contexts (Table S13).

401 These findings demonstrate that genetic ablation of cortistatin amplifies the
402 transcriptional response to cerebral ischemia, leading to exacerbated neuroinflammation,
403 compromised neurovascular remodelling and repression of responses critical for synaptic
404 function and recovery.

405 ***Lack of cortistatin exacerbates cellular imbalance following ischemic stroke***

406 To elucidate genotype-dependent cellular responses to cerebral ischemia, we employed
407 computational deconvolution of bulk transcriptomic data to infer brain cell-type composition in
408 the presence or absence of endogenous cortistatin. MGPs were employed to estimate the
409 relative abundance of neuronal, vascular, immune, and glial cell types (Fig. 3; Table S14).
410 Among neuronal populations, both genotypes exhibited a significant reduction in spiny neuron
411 signatures following MCAO, consistent with established features of ischemic injury [38].
412 Notably, a selective decrease in dentate granule neurons was observed exclusively in
413 cortistatin-deficient mice, indicating increased vulnerability of this neuronal subtype (Fig. 3a).
414 Ependymal neuron abundance increased in both genotypes post-ischemia, more prominently
415 in *Cort*$^{-/-}$ mice, potentially reflecting compensatory neurogenesis. Interestingly, GABAergic
416 interneuron populations (as cortistatin-expressing neurons), dopaminergic and NPC remained
417 unchanged following stroke (Fig. 3a). MGP analysis revealed that only *Cort*$^{-/-}$ mice had
418 significant increase in endothelial cells, pericytes, and vascular smooth muscle cells,
419 suggesting an amplified vascular response in the absence of cortistatin (Fig. 3a). This was
420 corroborated by GSEA enrichment (Fig. 3b). Both approaches also demonstrated that
421 signatures of CNS-associated macrophages, lymphocytes, monocyte-derived cells, and

422 neutrophils were enriched in the ischemic hemisphere of both genotypes, but were significant

423 only in *Cort*$^{-/-}$ mice, indicating heightened immune infiltration (Fig. 3a,b).

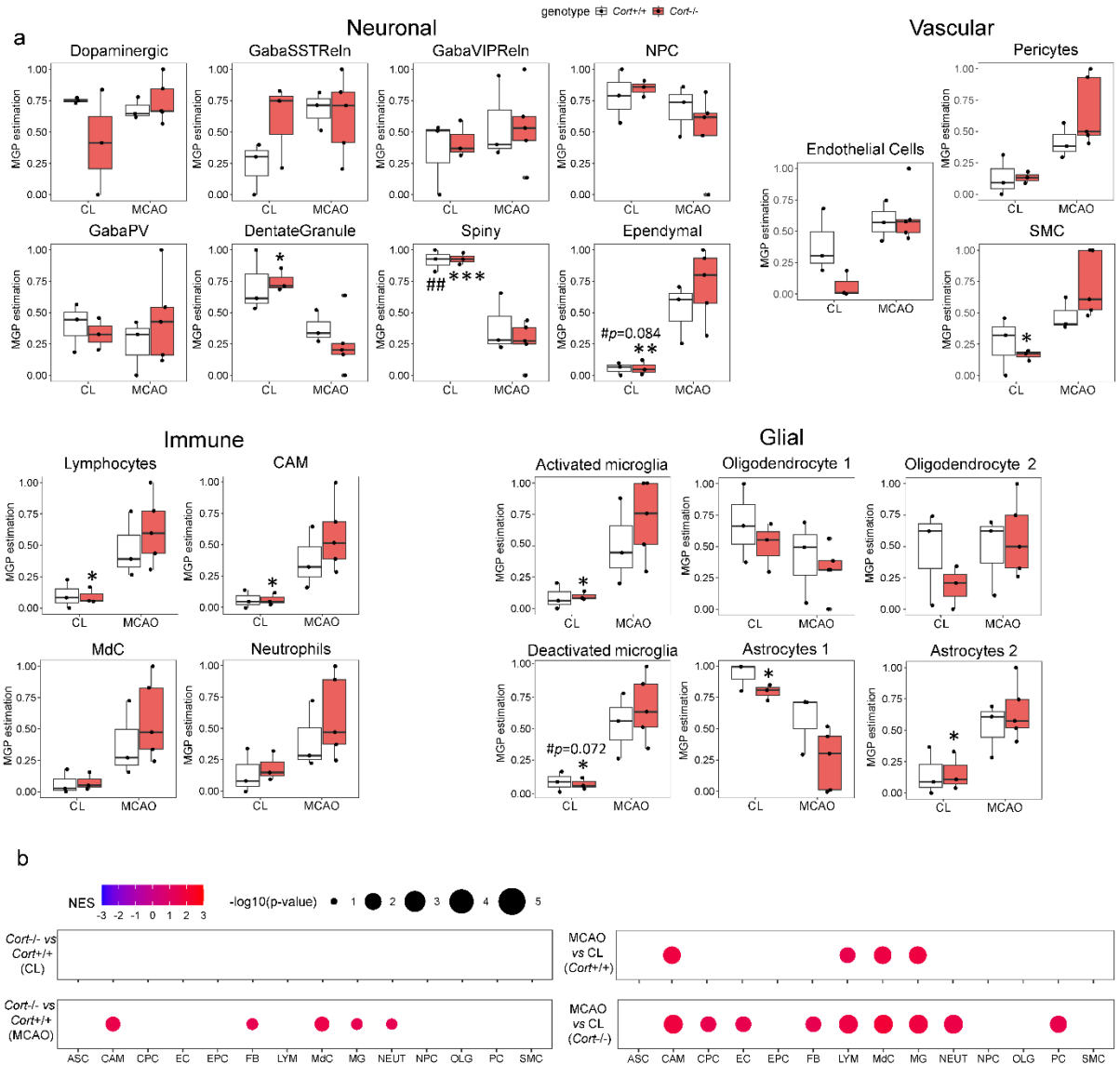

424

425 **Figure 3. Cortistatin deficiency alters brain cell proportions following ischemic stroke.** Cell-type-
426 specific gene expression patterns were identified by deconvolution of bulk RNA transcriptome data as
427 described in Methods. **a.** Boxplots display changes in cell-type composition between healthy (CL) and
428 ischemic (MCAO) hemispheres isolated from *Cort*$^{-/-}$ and *Cort*$^{+/+}$ animals 48h post-stroke. Marker gene
429 profile (MGP) analysis was used to infer cell population proportions. Cell types were grouped into four
430 main categories: neuronal (including dopaminergic, GABAergic-somatostatin (SST), GABAergic-
431 vasoactive intestinal peptide (VIP), and parvalbumin (PV)-expressing interneurons, neural progenitor
432 cells, and dentate granule, spiny and ependymal neurons), vascular (including endothelial cells,
433 pericytes, and smooth muscle cells), immune (including lymphocytes, central nervous system-
434 associated macrophages, monocyte-derived cells, and neutrophils) and glial cell types (including
435 microglia, astrocytes, and oligodendrocytes). **vs. Cort*$^{-/-}$ MCAO saline-treated mice, $^{\#}$*vs. Cort*$^{+/+}$ MCAO
436 saline-treated mice, $^{*/\#}p \leq 0.05$, $^{**/\#\#}p \leq 0.01$, $^{***/\#\#\#}p \leq 0.001$. **b.** Comparative GSEA performed using cell-
437 type–specific gene sets [29] between *Cort*$^{-/-}$ and *Cort*$^{+/+}$ in healthy *vs.* ischemic hemispheres (left) and
438 across ischemic progression within each genotype (right). Colour corresponds with Normalized
439 Enrichment Score (NES) and circle size indicates -log10(p-value). ASC: astrocyte, CAM: central

440 nervous system (CNS)-associated macrophage, CPC: choroid plexus capillary endothelial cell, EC:
441 endothelial cell, EPC: ependymocyte, FB: fibroblast, LYM: lymphocyte, MdC: monocyte-derived cell,
442 MG: microglia, NEUT: neutrophil, NPC: neural progenitor cell, OLG: oligodendrocyte, PC: pericyte,
443 SMC: vascular smooth muscle cell.
444
445 Analysis of glial cell populations demonstrated a significant increase in both activated
446 and deactivated microglial gene signatures in *Cort*$^{-/-}$ mice, that, together with peripheral
447 immune subsets, indicate a dysregulated neuroimmune response post-stroke. Astrocyte- and
448 oligodendrocyte-specific markers also revealed divergent phenotypes: a "Type 1" population
449 (based on markers from [29]) was significantly reduced in *Cort*$^{-/-}$ mice following MCAO,
450 whereas a "Type 2" profile (characterized by markers from [28], was significantly increased)
451 (Fig. 3a; Table S14).

452 Downregulation of astrocytic “Type 1” markers, typically associated with homeostatic
453 and neuroprotective functions, suggests a shift toward reactive or dysfunctional astrocyte
454 phenotypes in cortistatin-deficient mice following ischemia. Concurrent upregulation of the
455 “Type 2” profile indicates the emergence of a heterogeneous reactive astrocyte population
456 encompassing both neurotoxic and neuroprotective subsets. Although not statistically
457 significant, the oligodendrocyte profiles exhibited similar opposing trends in both genotypes:
458 decreased “Type 1” and increased “Type 2” signatures (Fig. 3a; Table S14). The elevated
459 “Type 2” profile likely reflects an injury-induced remyelination response, whereas the greater
460 reduction of “Type 1” markers in *Cort*$^{-/-}$ mice may denote impaired oligodendrocyte maturation
461 and myelin maintenance.

462 These findings underscore the critical role of cortistatin in preserving cellular
463 homeostasis post-stroke. Its deficiency drives broad dysregulation across neuronal, vascular,
464 immune, and glial compartments, fostering a pathological neuroimmune and neurovascular
465 environment that may hinder tissue repair and functional recovery.

466 ***Cortistatin deficiency exacerbates stroke-induced neurodegeneration, which is***
467 ***mitigated after cortistatin treatment***

468 To investigate the functional significance of endogenous cortistatin in stroke pathophysiology,
469 we subjected *Cort*$^{-/-}$ mice and age-matched wild-type mice to mild MCAO and assessed acute
470 neuropathological outcomes.

471 Our findings showed that cortistatin-deficient mice exhibited a greater propensity for
472 extensive infarcts, with 37.5% displaying lesions >30 mm^3, while >85% of *Cort*$^{+/+}$ animals
473 presented smaller lesions, as determined by CV staining (Fig. 4a,b; Table S15). MAP-2
474 immunostaining confirmed pronounced neuronal injury in *Cort*$^{-/-}$ mice, with >5 mm^2 MAP-2-
475 negative areas in 75% of animals, compared to only 22% wild-type controls (Fig. 4a,b; Table
476 S15). Furthermore, neurological impairment was significantly aggravated in *Cort*$^{-/-}$ mice, with
477 30% scoring 2-3 (persistent circling, severe motor incoordination, tremors), whereas all wild-
478 type mice remained below a score of 2 (intermittent severe motor incoordination, and tremors),
479 while all wild-type remained below a score of 2 (intermittent circling, moderate motor
480 incoordination, and mild hypomobility) (Figure 4c).

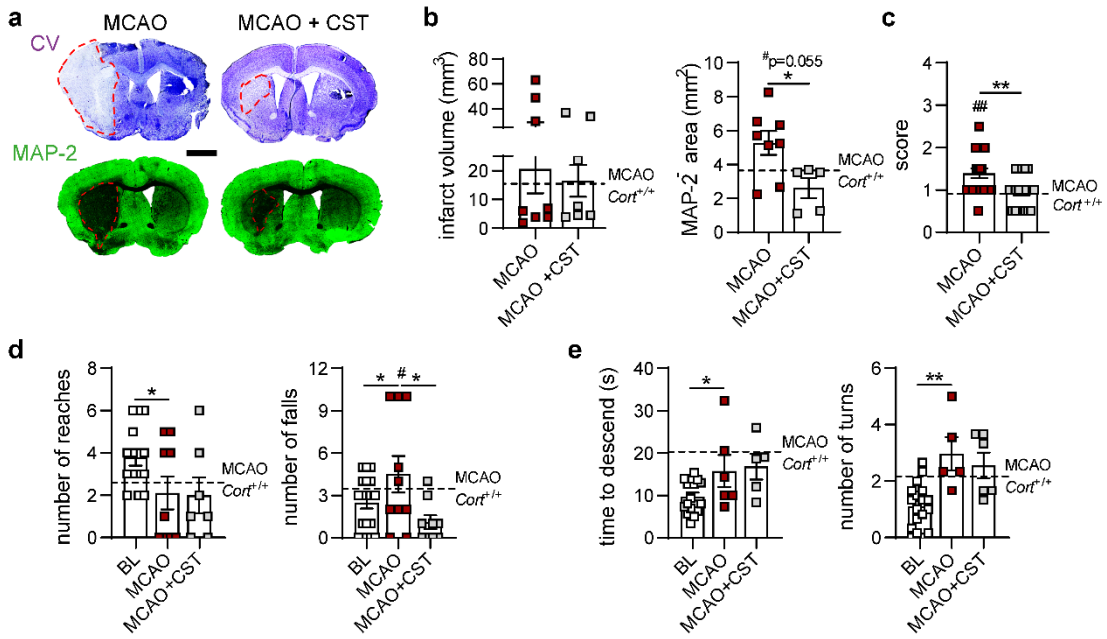

481 **Figure 4. Cortistatin deficiency worsens neuronal damage and neurological score, which are**
482 **ameliorated by cortistatin administration. a**. *Cort*$^{-/-}$ mice were subjected to MCAO and received either
483 saline (MCAO) or cortistatin (144µg/kg, MCAO+CST) 24h after reperfusion and were sacrificed 48h
484 post-surgery. Coronal brain sections were stained with cresyl violet (CV) (upper panel) or MAP-2 (lower
485 panel, green) to identify neuronal damage. Ischemic lesions are delineated by dashed red lines. Scale
486 bar: 1,500µm. **b**. Ischemic volume was quantified by measuring 10 CV-stained brain sections at 0.5
487 mm intervals per mouse (left) or by quantifying the lack of MAP-2 staining on coronal sections (right).
488 N=5-9 mice/group. **c**. Neurological scores were evaluated at 48h using a scale ranging from 0 (no signs)
489 to 3 (death). N=21-29 mice/group. **d-e.** Behaviour performances were assessed using wire-hanging

490 and pole tests, both at baseline (BL, pre-MCAO) and 48h post-MCAO. In the wire-hanging test (d), the
491 number of reaches towards one of the posts (left) and falls (right) were evaluated. N=7-10 mice/group.
492 In the pole test (e), the time to descend (s) (left) and the number of turns (right) until reaching the pad
493 were measured. N=5-6 mice/group. In b-e, comparisons were made to *Cort*$^{+/+}$ MCAO saline-treated
494 mice (dashed line). In d and e, BL, N=14-18 mice. Data are expressed as mean ± SEM with dots
495 representing individual mice. **vs*. *Cort*$^{-/-}$ MCAO saline-treated mice, $^{\#}$*vs*. *Cort*$^{+/+}$ MCAO saline-treated
496 mice, $^{*/\#}p \leq 0.05$, $^{**/\#\#}p \leq 0.01$. CST: cortistatin; MAP-2: microtubule-associated protein 2; MCAO:
497 middle cerebral artery occlusion.

498 Functional deficits were further evidenced by impaired performance in wire-hanging
499 and pole tests. Although post-stroke deficits were comparable between genotypes, cortistatin-
500 deficient mice displayed significantly more frequent falls (40% fell >5 times *vs.* none in wild-
501 type) and reduced success in reaching the post in the wire-hanging test (over 40% never
502 reached the post, whereas 80% of wild-type animals reaching at least once). Moreover, pole-
503 test performance was also impaired (Fig. 4d,e; Table S16).

504 Remarkably, administration of exogenous cortistatin to *Cort*$^{-/-}$ mice following MCAO
505 significantly ameliorated infarct size and neuronal injury, improved neurological score, and
506 restored motor outcomes to levels comparable with wild-type controls. Over 70% of treated
507 animals exhibited lesion volume <30 mm^3, none showed MAP-2-negative areas >5 mm^2, and
508 motor test performance was improved (Figure 4a-d; Table S16).

509 These results underscore the heightened vulnerability to ischemic stroke in the
510 absence of endogenous cortistatin and highlight its role in mitigating stroke-induced damage.

511 ***The neuroimmune response after stroke is dysregulated in cortistatin-deficient mice***
512 ***but becomes neuroprotective following cortistatin administration***

513 The neuroimmune response to stroke involves intricate and coordinated CNS-peripheral
514 immune interactions that shape both acute injury and long-term brain recovery [39].
515 Transcriptomic data previously revealed sustained neuroinflammation in cortistatin-deficient
516 mice post-stroke. However, the intrinsic role of cortistatin in systemic immune regulation is
517 unexplored. In this context, we found that, compared to wild-type mice, animals lacking
518 cortistatin exhibited significantly elevated serum IL-6 and MCP-1 levels post-MCAO,
519 accompanied by lymphopenia and reduced spleen mass, hallmarks of dysregulated peripheral
520 immunity (Fig. 5a,b). Administration of cortistatin normalized IL-6, elevated IL-12, and restored

521 both splenocyte count and spleen weight, indicating reestablishment of systemic immune

522 balance (Fig. 5a,b).

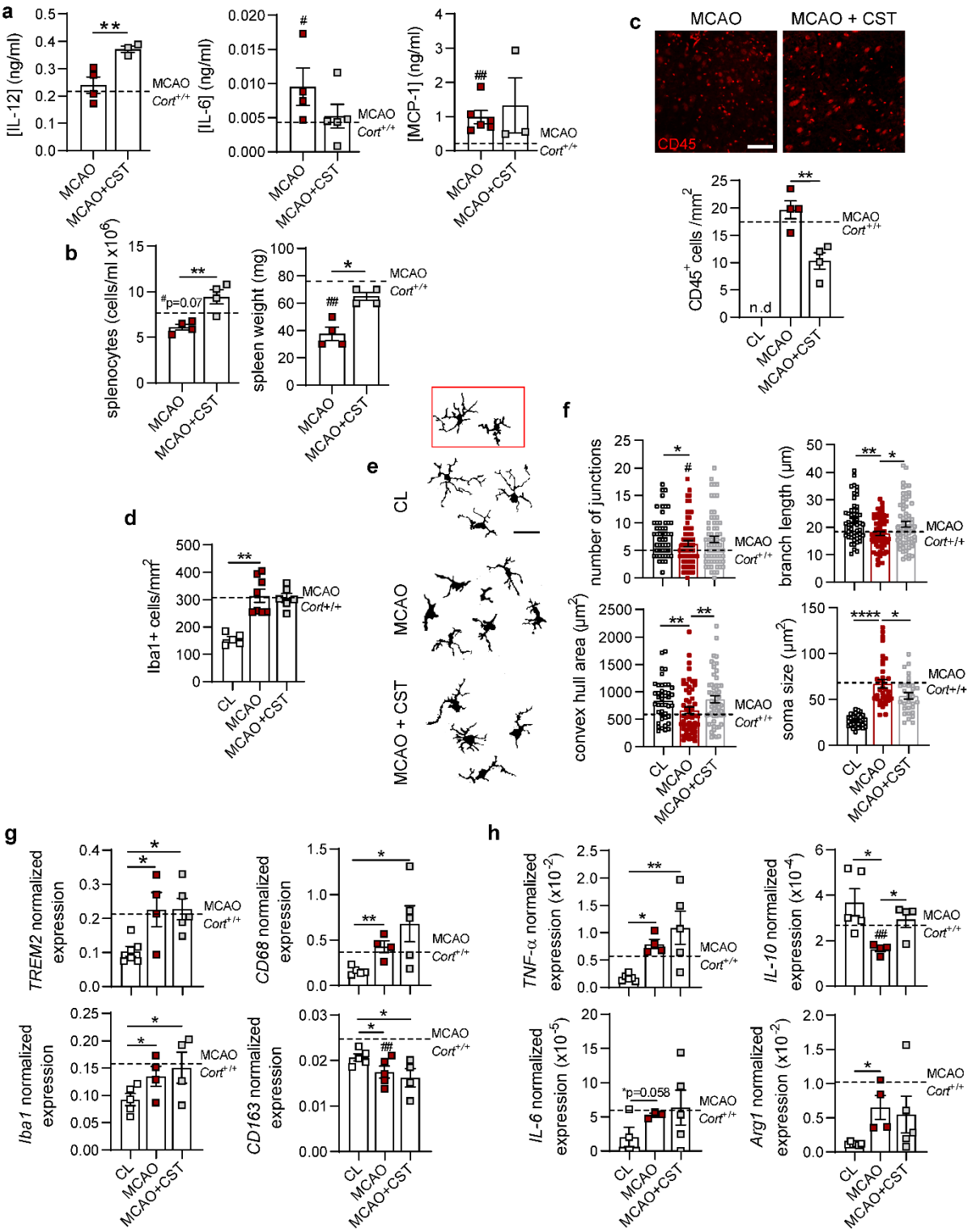

523

524 **Figure 5. Lack of cortistatin influences peripheral immunity and neuroinflammation post-stroke.**
525 MCAO was conducted in *Cort*$^{-/-}$ mice treated with either saline (MCAO) or cortistatin (144µg/kg)
526 (MCAO+CST) 24h after reperfusion and sacrificed at 48h. Mice were compared to *Cort*$^{+/+}$ MCAO saline-
527 treated mice (dashed line). **a**. Top, serum levels of IL-12, IL-6, and MCP-1 (ng/ml) were measured by

ELISA. IL-12: N=4 (MCAO *Cort*$^{-/-}$ mice), 3 (MCAO+CST *Cort*$^{-/-}$ mice); IL-6: N=4 (MCAO *Cort*$^{-/-}$ mice), 5 (MCAO+CST *Cort*$^{-/-}$ mice); MCP-1: N=6 (MCAO *Cort*$^{-/-}$ mice), 3 (MCAO+CST *Cort*$^{-/-}$ mice). **b.** Number of splenocytes/ml and spleen weight (mg). N=4 (MCAO and MCAO+CST *Cort*$^{-/-}$ mice). **c.** Top, representative CD45-stained (red) coronal sections showing leukocytes. Scale bar: 100µm. Bottom, leukocyte density (number of cells/mm^2) measured in the ischemic striatum (n.d: non-detected). **d.** Iba1+ population (cells/mm^2) measured in the contralateral (CL, uninjured) and ischemic core regions. **e.** Representative binarized microglia from CL or peri-lesion regions. Red rectangle represents *Cort*$^{+/+}$ MCAO saline-treated microglia. Scale bar: 30 µm. **f.** Iba1$^+$ cells morphology assessed using skeleton and fractal analysis. Skeleton: number of junctions and branch length: n=65 (MCAO *Cort*$^{-/-}$ mice and MCAO+CST *Cort*$^{-/-}$ mice) and n=50 (CL) cells from N=3 mice/group. Fractal: convex hull area n=55 (MCAO *Cort*$^{-/-}$ mice and MCAO+CST *Cort*$^{-/-}$ mice) and n=43 (CL hemisphere) cells from N=3 mice/group. Soma size was manually measured: n=35 (MCAO *Cort*$^{-/-}$ mice), n=30 (MCAO+CST *Cort*$^{-/-}$ mice), and n=31 (CL hemisphere) from N=3 mice/group. **g,h.** Gene expression of *Trem2, CD68, Iba1,* and *CD163* (**g**) and *TNF-α*, *IL-6*, *Arg1,* and *IL-10* (**h**) in CL and ipsilateral hemispheres of *Cort*$^{-/-}$ mice (MCAO saline vs. MCAO+CST), assessed by qPCR and normalized to *Rplp0*. N=4-6 mice/group. Wild-type MCAO values shown as a dashed line. Data: mean ± SEM; dots represent individual mice. **vs. Cort*$^{-/-}$ MCAO saline-treated mice, $^{\#}$*vs. Cort*$^{+/+}$ MCAO saline-treated mice. $^{*/\#}p \leq 0.05$, $^{**/\#\#}p \leq 0.01$, $^{***/\#\#\#}p \leq 0.001$. *Arg1*: arginase 1; *CD68*: cluster of differentiation 68; *CD163*: cluster of differentiation 163; CST: cortistatin; *Iba1*: ionized calcium-binding adaptor molecule 1; *IL-6*: interleukin 6; *IL-1β*: interleukin 1β; *IL-10*: interleukin 10; IL-12: interleukin 12; MCAO: middle cerebral artery occlusion; *MCP-1*: Monocyte Chemoattractant Protein- 1; *TNF-α*: tumour necrosis factor-α; *Trem2*: triggering receptor expressed on myeloid cells 2.

In the brain, elevated densities of CD45$^+$ and Iba1$^+$ myeloid cells were observed in the infarct core of cortistatin-deficient mice, paralleling wild-type levels (Fig. 5c,d). However, cortistatin deficiency exacerbated myeloid cell activation post-stroke. Compared to contralateral hemisphere, Iba1$^+$ cells from mice lacking cortistatin displayed a reactive morphology, characterized by reduced branching, shorter processes, increased soma size, and diminished territory area, suggesting enhanced activation (Fig. 5e,f). Gene expression analysis revealed similar upregulation of both pro- and anti-inflammatory markers between genotypes (*Trem2, CD68, Iba1 TNF-α*, *IL-6* and *Arg1*), though *Cort*$^{-/-}$ mice showed significantly reduced *CD163* and *IL-10* expression, indicative of impaired anti-inflammatory responses (Fig. 5g,h). Cortistatin administration selectively reduced CD45$^+$ cells without affecting Iba1$^+$ cells, suggesting distinct regulatory mechanisms. In fact, cortistatin treatment promoted a shift toward a more ramified Iba1$^+$ phenotype with increased IL-10, supporting a reparative glial response distinct from MCAO wild-type profiles (Fig. 5f-h).

Astrocyte responses were similarly disrupted in cortistatin-deficient mice, with reduced glial scar formation and atypical astrocyte morphologies compared to wild-type animals (smaller soma, fewer and shorter processes and elongated morphology, increased span ratio, and reduced territorial coverage) (Fig. 6a,b). Additionally, GFAP expression, upregulated after

567 MCAO, was significantly lower in cortistatin-deficient mice, accompanied by reduced BDNF
568 and GDNF (Fig. 6c). Notably, cortistatin treatment markedly restored astrocytic morphology
569 and function and increased GDNF expression to similar levels seen in wild-type MCAO mice
570 (Fig. 6c).

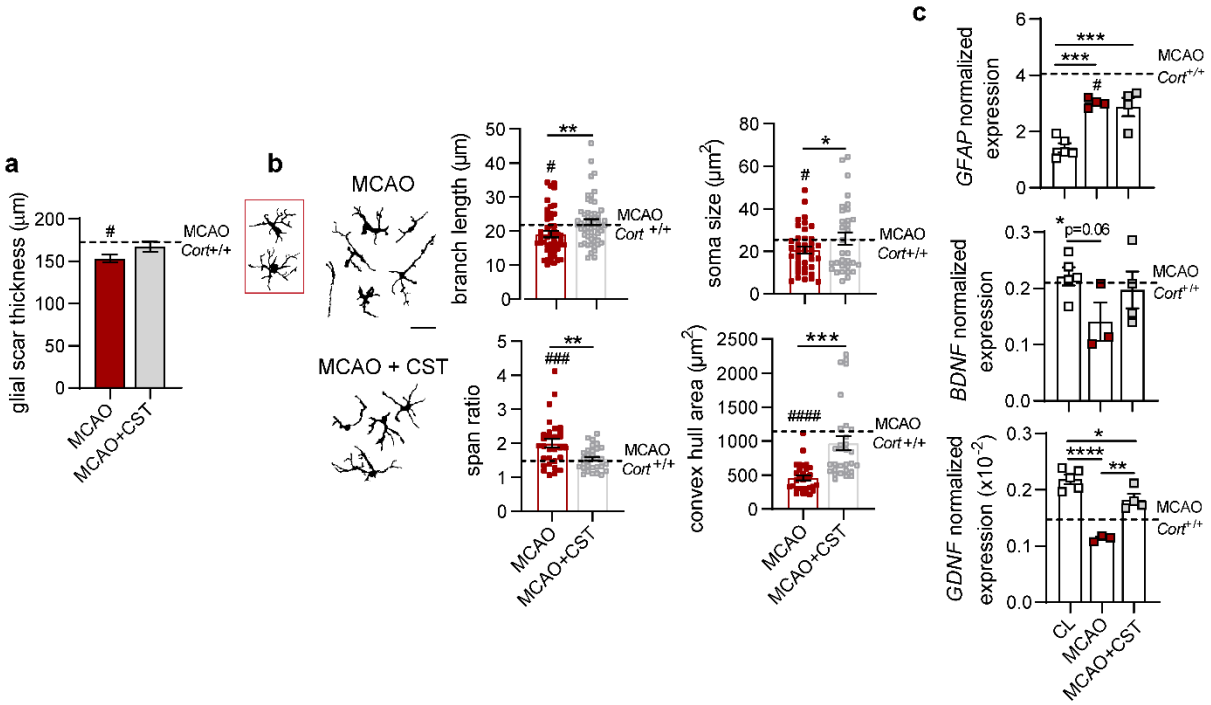

571

572 **Figure 6. Lack of cortistatin impairs astrocytic function post-stroke, which is restored after**
573 **cortistatin treatment**. MCAO was conducted in *Cort*$^{-/-}$ mice treated with either saline (MCAO) or
574 cortistatin (144µg/kg) (MCAO+CST) 24h after reperfusion. Animals were sacrificed at 48h. Mice were
575 compared to *Cort*$^{+/+}$ MCAO saline-treated mice (dashed line). **a.** Glial scar thickness was quantified.
576 n=57 (MCAO *Cort*$^{-/-}$ mice) and n=54 (MCAO+CST *Cort*$^{-/-}$ mice), ROIs from N=4 mice/group. **b.** Left,
577 representative binary images of astrocytes were extracted from the glial scar. Scale bar: 30µm. Right,
578 evaluation of morphological parameters of astrocytes. Branch length was evaluated by skeleton
579 analysis: n=49 (MCAO *Cort*$^{-/-}$ mice), n=57 (MCAO+CST *Cort*$^{-/-}$ mice) cells from N=3 mice/group. Soma
580 size was manually measured: n=39 (MCAO *Cort*$^{-/-}$ mice), n=32 (MCAO+CST *Cort*$^{-/-}$ mice) cells from N=3
581 mice/group. Span ratio and cell territory (convex hull area) were analysed by fractal analysis. n=30 cells
582 from N=3 mice/group. **c.** Gene expression levels of *GFAP*, *BDNF,* and *GDNF* in the contralateral (CL,
583 uninjured) and ipsilateral (ischemic) brain hemispheres of *Cort*$^{-/-}$ mice treated with saline or cortistatin
584 following MCAO, were analysed by real-time qPCR and normalized to *Rplp0* expression. N=3-5
585 mice/group. Data represent the mean ± SEM. **vs. Cort*$^{-/-}$ MCAO saline-treated mice, $^{\#}$*vs. Cort*$^{+/+}$ MCAO
586 saline-treated mice, $^{*/\#}p \leq 0.05$, $^{**/\#\#}p \leq 0.01$, $^{***/\#\#\#}p \leq 0.001$. *BDNF*: brain-derived neurotrophic factor;
587 CST: cortistatin; *GDNF:* glial-derived neurotrophic factor; *GFAP*: glial fibrillary acidic protein; MCAO:
588 middle cerebral artery occlusion.

589 Together, these findings demonstrate that cortistatin is essential for maintaining
590 neuroimmune and glial homeostasis after stroke. Cortistatin deficiency drives excessive
591 peripheral and central immune activation, coupled with dysfunctional glial responses, thereby

592 amplifying neuronal injury. Conversely, exogenous cortistatin reprograms both systemic and
593 CNS immune compartments toward reparative phenotypes.

594 ***Cortistatin deficiency affects BBB integrity and vascular dynamics after ischemic***
595 ***stroke, which are normalized following cortistatin administration***

596 Given previous evidence of enhanced BBB permeability in cortistatin-deficient mice under
597 systemic inflammation [14], we investigated BBB dynamics post-stroke. Following MCAO,
598 cortistatin-deficient mice exhibited significantly elevated parenchymal IgG accumulation
599 relative to wild-type controls, indicative of substantial BBB disruption (Fig. 7a). This
600 permeability likely contributes to the enhanced immune cell infiltration previously observed
601 (Fig. 5c). Analysis of TJ and vascular markers revealed that, while C*laudin-5* expression
602 remained unchanged and similar to the expression previously found in wild-type mice [15],
603 and comparable vessel density and diameter between genotypes post-MCAO were observed,
604 C*laudin-1*, *Occludin*, and *Col1a2* levels were significantly reduced in the ischemic hemisphere
605 of cortistatin-deficient mice (Fig. 7b,d). ZO-1 distribution was also disrupted, with notable loss
606 across the endothelium (Fig. 7c). These alterations reflect compromised TJ architecture and
607 endothelial integrity. Administration of cortistatin significantly reduced IgG leakage, normalised
608 *Claudin-1* and *Occludin* expression, and normalised ZO-1 localization, thereby attenuating
609 BBB disruption (Fig. 7a-c). In addition, cortistatin treatment promoted vascular remodelling,
610 evidenced by increased vessel area and diameter within the ischemic striatum (Fig. 7d). These
611 results indicate that cortistatin deficiency exacerbates BBB breakdown and impairs vascular
612 stability, while exogenous cortistatin promotes barrier integrity and vascular resilience.

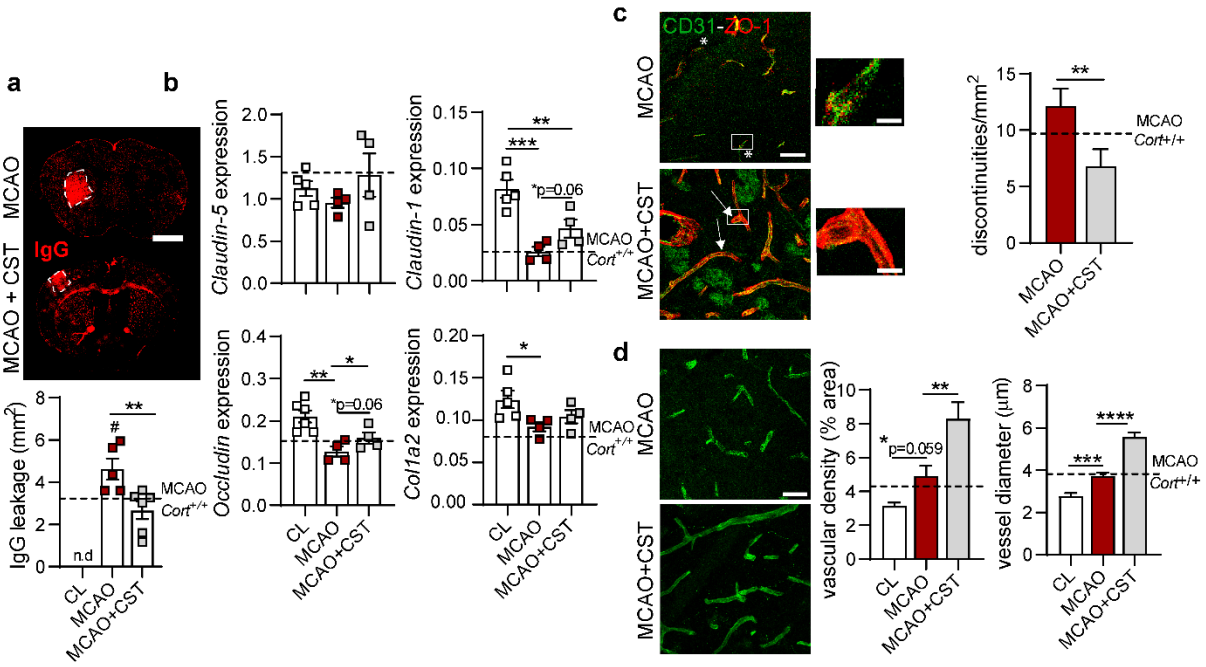

Figure 7. Absence of cortistatin exacerbates BBB breakdown, which is ameliorated by cortistatin administration. a. Top, coronal brain sections from *Cort*$^{-/-}$ mice treated with either saline (MCAO) or cortistatin (144µg/kg) (MCAO+CST) at 24h post-reperfusion and sacrificed at 48h. Sections were stained with a fluorescently labelled antibody against mouse IgGs. Regions of IgG leakage are indicated with dashed white lines. Scale bar: 1,500µm. Quantification of IgG^{+} areas (bottom) was used to assess IgG leakage from the blood. N=5-6 mice/group. **b.** Gene expression levels of C*laudin-5, Claudin-1, Occludin*, and *Col1a2* in the contralateral (CL) and ipsilateral brain hemispheres were quantified by real-time qPCR and normalized to *Rplp0* expression. Gene expression levels of wild-type mice are depicted as a dashed line as a reference. N=4-5 mice/group. **c.** Left, representative images of the ipsilateral striatum from *Cort*$^{-/-}$ mice post-MCAO and treated with cortistatin, stained with CD31 antibody for brain endothelial cells (BECs, green) and ZO-1 (red) for TJs. Scale bar: 30µm. Detailed images with ZO-1 discontinuities (indicated by asterisks) and recovery of ZO-1 coverage (marked with arrows) are shown. Scale bar of magnifications: 120µm. Right, quantification of the number of ZO-1 discontinuities per vessel area. n=2 ROIs/mouse; N=3-6 mice/group. **d.** Left, representative images of the ipsilateral striatum of *Cort*$^{-/-}$ mice following MCAO and treated with cortistatin, stained with CD31 antibody for BECs (green). Scale bar: 30µm. Right, vascular density was calculated as the percentage of CD31-positive staining relative to the total image area. n=3 ROIs/mouse; N=3-4 mice/group. Vessel diameter was measured manually and quantified on different sections from each vessel from 5-10 vessels/mouse, N=3-4 mice/group. Mice were compared to *Cort*$^{+/+}$ MCAO saline-treated mice (dashed line). Data represent the mean ± SEM. **vs. Cort*$^{-/-}$ MCAO saline-treated mice, *#vs. Cort*$^{+/+}$ MCAO saline-treated mice, $^{*/\#}p \leq 0.05$, $^{**/\#\#}p \leq 0.01$, $^{***/\#\#\#}p \leq 0.001$, $^{****/\#\#\#\#}p \leq 0.0001$. CD31: cluster of differentiation 31; CL: contralateral; *Col1a2*: collagen type I; CST: cortistatin; IgG: immunoglobulin G; MCAO: middle cerebral artery occlusion; ZO-1: zonula-occludens 1.

Absence of cortistatin impacts subacute stroke outcome while exogenous treatment potentiates recovery

Regarding the role of cortistatin in acute stroke, and following STAIR recommendations [40,41], we extended our analysis to the early subacute phase (7 days post-MCAO), focusing on key markers of injury and recovery. While neurological deficit scores were initially comparable between genotypes (Fig. 8a), animals lacking cortistatin exhibited trends toward

643 larger infarcts, greater MAP-2-negative areas, and reduced neuronal density relative to wild-
644 type controls (Fig. 8b; Table S15; Fig. S4a). Functional impairments persisted in *Cort*$^{-/-}$ mice,
645 including decreased successful reaches and poorer wire-hanging test performance, although
646 pole test results remained unaffected (Fig. S5a,b; Table S16). Histological analysis revealed
647 pronounced axonal disorganization and aberrant myelin structures in *Cort*$^{-/-}$ mice, reflected by
648 elevated MBP intensity in the ischemic hemisphere, suggestive of myelin disruption [42] (Fig.
649 8c). Cortistatin treatment ameliorated these pathological alterations, improving neuronal
650 density, axonal integrity, and neurological scores in both genotypes (Fig. 8a-c).

651

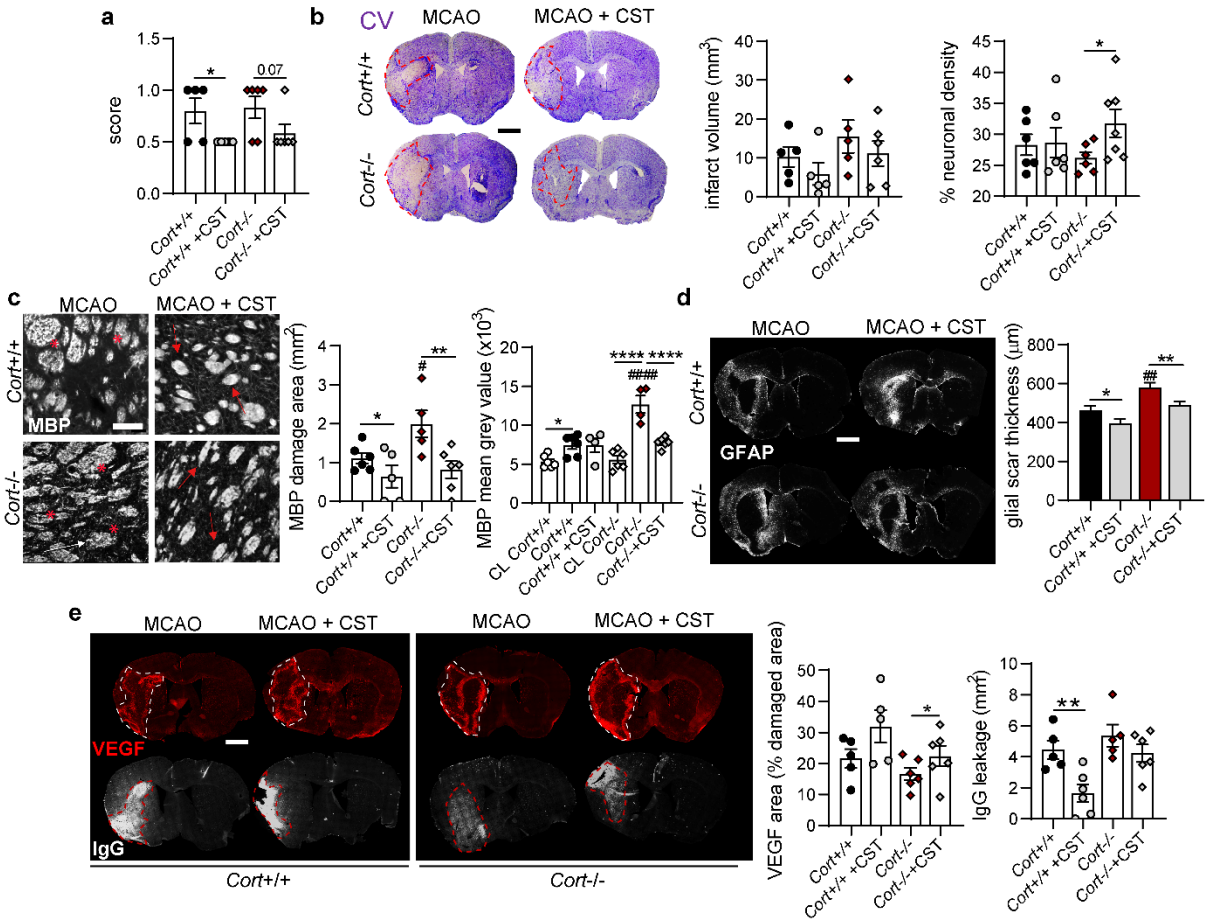

652

653 **Figure 8. Cortistatin deficiency impairs long-term stroke recovery, while treatment improves**
654 **outcomes**. *Cort*$^{+/+}$ and *Cort*$^{-/-}$ mice were treated daily with either saline (MCAO) or cortistatin (144µg/kg)
655 (MCAO+CST), from 24h post-reperfusion, and sacrificed at 7 days. **a.** Neurological scores were
656 evaluated at 7 days using a scale ranging from 0 (no signs) to 3 (death). N=5-6 mice/group. **b.** Left,
657 brain coronal sections were stained with cresyl violet (CV) to assess neuronal damage. Ischemic lesions
658 are outlined with dashed red lines. Scale bar: 1,500µm. Centre, ischemic volume was determined by
659 analysing ten CV-stained brain slices at 0.5 mm intervals per mouse. Right, neuronal density within the

660 ischemic area was quantified (% of total area). N=4-6 mice/group. **c.** Left, representative images of the
661 ipsilateral striatum stained with MBP antibody to visualize myelin sheaths. Aberrant myelin sheaths are
662 depicted with asterisk while recovered ones are marked with arrows. Scale bar: 30µm. Right, the area
663 of damaged myelin sheaths (left) and MBP mean grey value (right) were quantified. N=4-6 mice/group.
664 **d.** Left, representative brain sections stained with GFAP antibody to identify astrocytes. Scale bar:
665 1,500µm. Right, glial scar thickness was quantified. N=4-6 mice/group. **e.** Left, sections were stained
666 with VEGF antibody (red) and with a fluorescently-labelled antibody against mouse IgGs (white). Scale
667 bar: 1,500µm. Centre, $VEGF^+$ area was quantified as the % of positive area within the damaged area.
668 N=4-6 mice/group. Right**,** IgG^+ area was measured to assess BBB leakage. N=4-6 mice/group. Data
669 represent the mean ± SEM. **vs.* MCAO cortistatin-treated mice, *#vs. Cort*$^{+/+}$ MCAO saline-treated mice,
670 $^{*/\#}p \leq 0.05$, $^{**/\#\#}p \leq 0.01$, $^{****/\#\#\#\#}p \leq 0.0001$. BBB: blood-brain barrier, CST: cortistatin, GFAP: glial
671 fibrillary acidic protein, Iba1: ionized calcium-binding adaptor molecule 1, IgG: immunoglobulin G, MBP:
672 myelin basic protein, MCAO: middle cerebral artery occlusion.

673 Glial responses were also altered in the subacute phase. Iba1+ cell density increased
674 substantially compared to acute timepoints (>10^3 cells/mm^2 *vs.* <400 cells/mm^2) with no
675 genotype- or treatment-dependent differences (Fig. 5d; Fig. S4b). Similarly, glial scar
676 thickness augmented as the stroke progressed (<200 to >400 µm from acute to subacute
677 stroke) (Fig. 6a,8d), with *Cort*$^{-/-}$ mice transitioning from disorganized to significantly fibrotic
678 thicker scars at 7 days (Fig. 6a,8d). Cortistatin treatment reduced scar thickness in both
679 genotypes, suggesting a role in regulating scar maturation. Additionally, cortistatin
680 administration upregulated VEGF expression in the ischemic hemisphere, potentially
681 enhancing angiogenesis and BBB repair (Fig. 8e). Consistently, IgG extravasation was
682 reduced following treatment, aligning with observations at earlier stages (Fig. 7a, Fig. 8e).

683 These findings demonstrated that cortistatin deficiency worsens subacute stroke
684 pathology, hindering neurovascular and glial repair, accordingly to transcriptomic studies
685 showing limited activation of repairing pathways in the ischemic brain without cortistatin.
686 Exogenous cortistatin reversed many of these pathological features, underscoring its broad
687 neurorepair potential beyond the acute phase.

688 ***Cortistatin regulates neuroinflammatory and vascular outcomes after stroke in middle-***
689 ***aged mice***

690 To evaluate the influence of cortistatin on stroke outcome in the context of aging, we induced
691 mild MCAO in middle-aged (6-month-old) *Cort*$^{+/+}$ and *Cort*$^{-/-}$ mice, with or without cortistatin
692 treatment, and compared results to young (3-month-old) MCAO animals.

693 In the acute phase, cortistatin deficiency in middle-aged mice led to worsened
694 neurological scores and behavioural deficits, paralleling findings in younger cohorts (Fig. 9a;
695 Fig. S5c,d). Neuronal damage, as indicated by MAP-2 loss, was greater in older wild-type
696 mice, a difference not observed in *Cort*$^{-/-}$ animals (Fig. 9b; Table S15). Cortistatin treatment
697 reduced neuronal injury in wild-type mice and led to an improved score in cortistatin-deficient
698 mice (Fig. 9a,b). Additionally, cortistatin improved pole test outcomes, though it demonstrated
699 generally limited effect (Fig. S5c,d; Table S16).

700 Glial analysis revealed increased Iba1^{+} cell density and a hyper-ramified phenotype in
701 the ischemic hemisphere of middle-aged *Cort*$^{-/-}$ mice, with exacerbation of age-dependent
702 features relative to young animals (Fig. 9c-g). Cortistatin administration restored a
703 homeostatic microglial morphology in both genotypes. Astrocytic responses were also
704 impaired in middle-aged *Cort*$^{-/-}$ mice, marked by disrupted glial scars and atypical astrocyte
705 morphology (fewer junctions, reduced branching, and diminished territorial complexity), which
706 were normalized following cortistatin administration (Fig. 9h-l).

707 Assessment of BBB integrity revealed no age-related differences in IgG extravasation
708 within genotypes; however, *Cort*$^{-/-}$ mice exhibited significantly greater leakage than wild-type
709 counterparts. (Fig. 10a). This disruption was accompanied by reduced vascular density in
710 middle-aged *Cort*$^{-/-}$ mice (Fig. 10b). Cortistatin administration ameliorated BBB leakage and
711 regulated vascular remodelling in both genotypes, consistent with findings in younger mice
712 (Figs. 10a,b; Fig. 7a). Although ZO-1 disruption was similarly reduced with aging, cortistatin
713 preserved junctional organization, particularly in wild-type mice (Fig. 10c). Increased BBB
714 permeability in cortistatin-deficient mice correlated with greater immune cell infiltration, which
715 was also reversed following cortistatin treatment (Fig. 10d).

716 Notably, aging amplified the systemic immune response to stroke, with elevated IL-12,
717 IL-6, and MCP-1, particularly in the absence of cortistatin (Fig. S6). Cortistatin treatment
718 significantly attenuated these inflammatory mediators across genotypes.

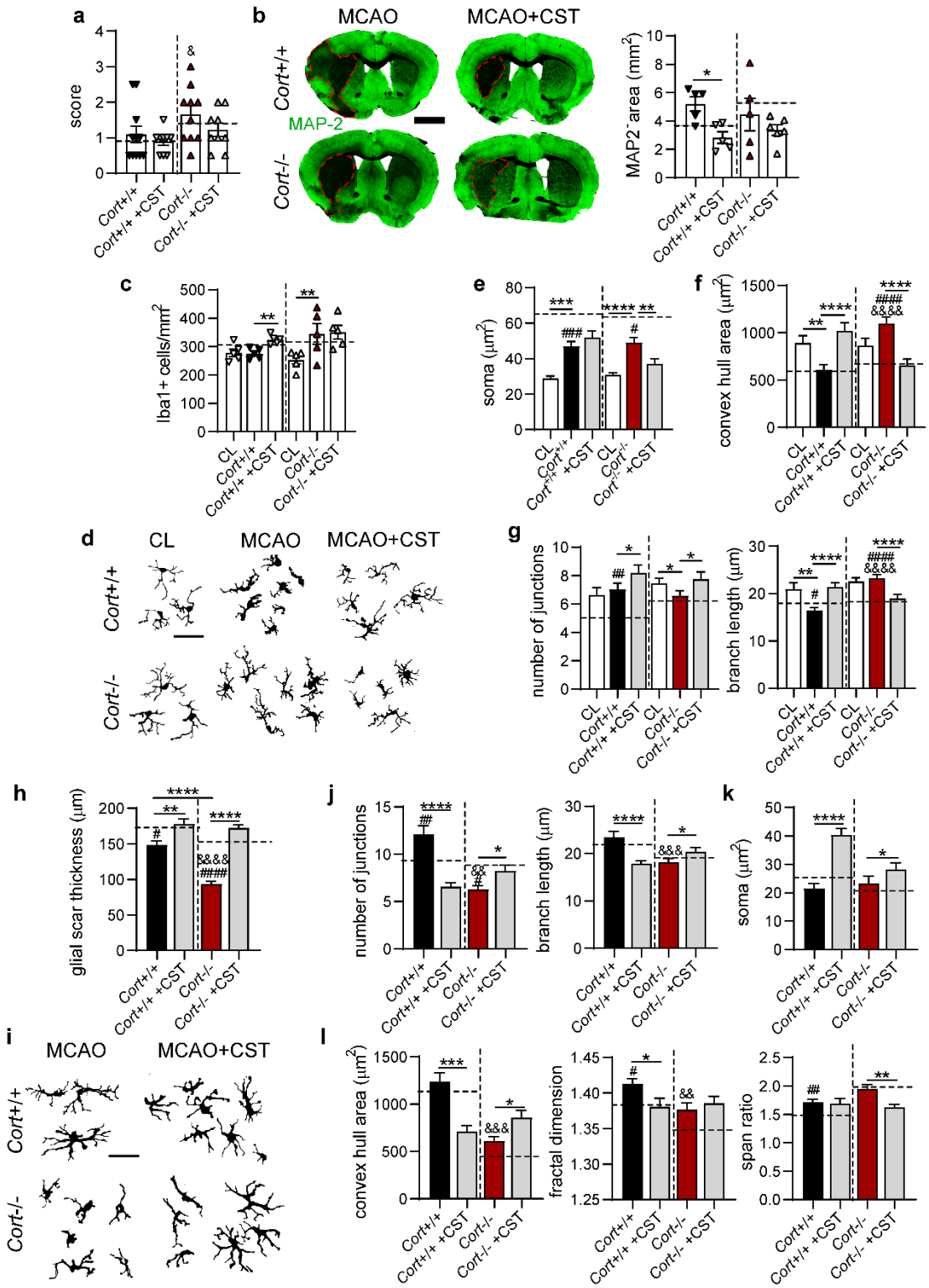

Figure 9. Lack of cortistatin exacerbates stroke outcomes and glial dysregulation in middle-aged mice. 6-month-old *Cort*$^{+/+}$ and *Cort*$^{-/-}$ mice were subjected to middle cerebral artery occlusion and treated with either saline (MCAO) or cortistatin (144µg/kg, MCAO+CST) at 24h post-reperfusion and sacrificed at 48h. **a.** Neurological deficits were scored from 0 (no signs) to 3 (death). N=9-12 mice/group. **b**, Left, microtubule-associated protein 2 immunostaining (MAP-2, green) highlights ischemic areas (red dashed lines). Scale bar: 1,500µm. Right, neuronal integrity was evaluated by measuring MAP-2 loss. N=5–6 mice per group. **c.** Iba1^{+} population (cells/mm²) was quantified in contralateral (CL) and ischemic core regions. **d.** Binary images of Iba1+ cells from CL and peri-lesion. Scale bar: 30µm. **e–g.**

Quantification of Iba1⁺ microglial morphology: soma size, manually measured (**e**), convex hull area, evaluated by fractal analysis (**f**), and junction number and branch length, determined by skeleton analysis (**g**). Cell counts per group: n=30-35 cells, N=3 mice/group. **h.** Glial scar thickness was quantified, n=30-35 ROIs, N=3 mice/group. **i.** Representative binary images of glial scar astrocytes. Scale bar: 30µm. **j–l.** Astrocyte morphological features analysed via skeleton and fractal analysis: junctions and branching, (**j**), soma size (**k**), and convex hull area, fractal dimension and span ratio (**l**). Cell counts per group: n=30-35 cells, N=3 mice/group. Data were compared to MCAO saline-treated young *Cort*$^{+/+}$ and *Cort*$^{-/-}$ mice (dashed line). Data are expressed as mean ± SEM. **vs. Cort*$^{+/+}$ or *Cort*$^{-/-}$ MCAO saline-treated mice; *#vs.* young *Cort*$^{+/+}$ or *Cort*$^{-/-}$ MCAO saline-treated mice; *&vs.* middle-aged *Cort*$^{+/+}$ MCAO saline-treated mice */#/&$p \leq 0.05$. */#/&$p \leq 0.05$, **/##/&&$p \leq 0.01$, ***/###/&&&$p \leq 0.001$, ****/####/&&&&$p \leq 0.0001$. CST, cortistatin; MCAO, middle cerebral artery occlusion.

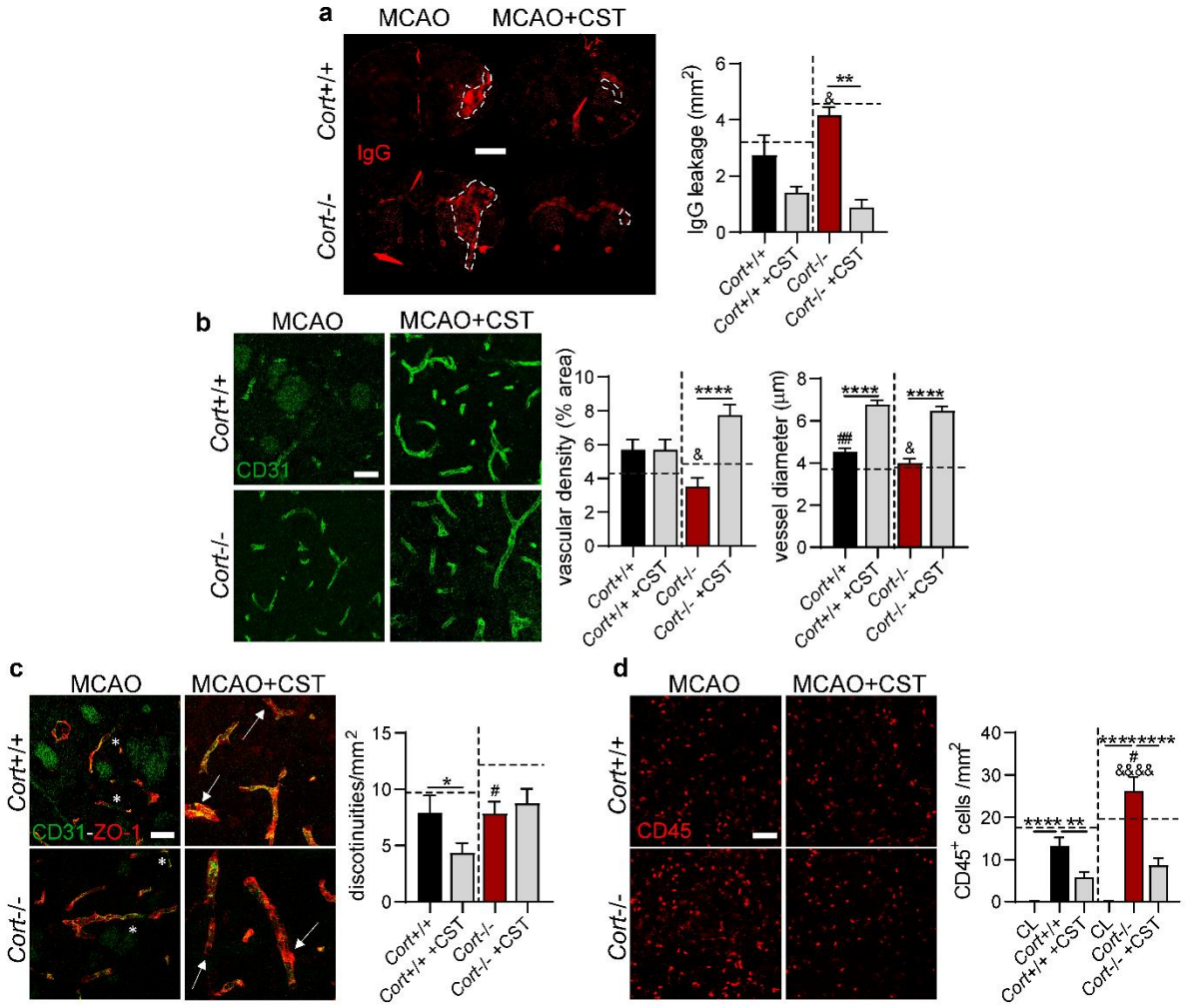

Figure 10. Middle-aged cortistatin-deficient mice display disrupted vascular integrity following ischemic stroke. 6-month-old *Cort*$^{+/+}$ and *Cort*$^{-/-}$ mice were subjected to middle cerebral artery occlusion (MCAO) and treated with either saline (MCAO) or cortistatin (144µg/kg, MCAO+CST) at 24h post-reperfusion and sacrificed at 48h. **a.** Left, representative brain sections stained with a fluorescently labelled antibody against mouse IgG. Areas of IgG extravasation are outlined with dashed white lines. Scale bar: 1,500µm. Right, IgG⁺ area was quantified to assess BBB permeability. N=4–6 mice/group. **b.** Left, representative images of the lesion core (striatum) stained with CD31 antibody (green) to visualize BECs. Scale bar: 30µm. Right, quantification of vascular integrity, including vascular density (percentage of CD31⁺ staining per total image area, left) and vessel diameter (manually measured and quantified in different sections from each vessel from 5-10 vessels/mouse, right). N=3–6 mice/group. **c.** Left, representative images of the ipsilateral striatum stained with CD31 (green) and zonula occludens-1 (ZO-1, red) to assess TJ integrity. ZO-1 discontinuities are marked with asterisks, while areas of ZO-1 uniformity are indicated by arrows. Scale bar: 30µm. Right, quantification of the number of ZO-1 discontinuities per vessel area. n=3 ROIs/section/mouse; N=3–5 mice/group. **d.** Left, high-magnification

754 images of the striatum stained with CD45 antibody (red) to detect infiltrating leukocytes. Scale bar:
755 100µm. Right, leukocyte density (cells/mm²) was quantified in the ischemic striatum and the
756 contralateral hemisphere (CL, uninjured). Data were compared to young *Cort*$^{+/+}$ and *Cort*$^{-/-}$ mice
757 subjected to MCAO and treated with saline (dashed line). Data are presented as mean ± SEM. **vs*.
758 MCAO cortistatin-treated mice; $^{\#}$*vs*. middle-aged *Cort*$^{+/+}$ MCAO saline-treated mice; $^{\&}$*vs*. young *Cort*$^{+/+}$
759 or *Cort*$^{-/-}$ MCAO saline-treated mice. $^{*/\#/\&}p \leq 0.05$, $^{**/\#\#/\&\&}p \leq 0.01$, $^{***/\#\#\#/\&\&\&}p \leq 0.001$, $^{****/\#\#\#\#/\&\&\&\&}p \leq$
760 0.0001. CD31, cluster of differentiation 31; CD45, cluster of differentiation 45; CST, cortistatin; IgG,
761 immunoglobulin G; MCAO, middle cerebral artery occlusion; TJ, tight-junction; ZO-1, zonula occludens-
762 1.

763 In summary, cortistatin deficiency exacerbates age-associated neuroinflammatory
764 responses, glial and vascular dysfunction, and peripheral immune activation following
765 ischemia. Exogenous cortistatin confers robust neurovascular protection and immune
766 regulation in both young and middle-aged mice, supporting its therapeutic potential across
767 age groups.

768 **DISCUSSION**

769 Stroke pathogenesis involves complex neurovascular-immune interactions shaped by spatial
770 and temporal dynamics influencing both injury and recovery [4]. Moreover, current stroke
771 research often relies on oversimplified preclinical models that overlook variables such as
772 aging, comorbidities, and chronic outcomes. This challenges therapy development,
773 contributing to stroke being the second leading cause of mortality worldwide. Thus,
774 understanding temporal multi-system interactions, along with their endogenous mediators, is
775 critical for advancing stroke management.

776 In this study, we identified cortistatin as a critical neuroimmune regulator in stroke
777 pathophysiology. Integrative transcriptomic analysis across human and murine datasets,
778 covering various tissues, models, and stroke phases, consistently revealed its significant
779 downregulation post-stroke. Indeed, recent studies identify cortistatin as a DEG in ischemic
780 mouse brain [43,44], underscoring a conserved involvement in the response to cerebral
781 ischemia. The inverse association between cortistatin levels and stroke severity further
782 suggests that reduced cortistatin is not merely a consequence of injury but may actively
783 contribute to disease progression and its (timely) administration may help protect against
784 ischemic stroke.

785 To test this hypothesis, we investigated for the first time the endogenous role of
786 cortistatin in a preclinical stroke model (MCAO) in young and middle-aged cortistatin-deficient
787 mice. Considering their known heightened susceptibility to other neural injury experimental
788 approaches [45–48], we selected a mild stroke model which confers advantages such as a
789 lower mortality rate and reduced endothelial injury, yielding more consistent infarct sizes [49].
790 In this context, we assessed both acute and subacute outcomes while evaluating the potential
791 therapeutic efficacy of cortistatin in reversing pathological phenotypes.

792 Our *in vivo* experiments showed that cortistatin-deficient mice had an exacerbated
793 molecular and cellular response to ischemia compared to wild-type mice. While both
794 genotypes exhibited upregulation of immune activation, inflammation, and tissue remodelling
795 related-genes, these responses were significantly amplified in the absence of cortistatin.
796 Moreover, cortistatin deficiency was related to heightened neuroinflammation, neurovascular
797 dysfunction, and impaired synaptic processes, transcriptional signatures of maladaptive post-
798 ischemic responses that drive secondary injury, impede regeneration, and contribute to poor
799 stroke outcomes [50]. According to this, our findings revealed worse neurological scores, in
800 young and middle-aged cortistatin-deficient mice during the acute stroke stage, compared to
801 wild-type animals. This agreed with the larger lesions in young cortistatin-deficient mice at
802 acute and subacute phases, suggesting a pivotal role for cortistatin in neuronal survival after
803 injury. Surprisingly, while lesion size increased with age in wild-type mice, it remained stable
804 in cortistatin-deficient animals, consistent with evidence that infarct size does not always
805 match neurological outcomes [51–53]. Furthermore, a greater proportion of cortistatin-
806 deficient mice showed impaired performance in behavioural tests at both ages, though their
807 motor performance was not consistently worse despite greater neurological deficits. This
808 underlines the heterogeneity of behavioural stroke phenotypes and the need for
809 comprehensive assessment using complementary functional tests [53]. Additionally, using a
810 mild stroke model with uniform manifestations may limit direct correlations between lesion size
811 and functional deficits [54]. Moreover, the heightened anxiety-like behaviour of deficient mice,

812 previously described by our group, driven by elevated glucocorticoid levels observed in the
813 absence of cortistatin [9], may influence behaviour and mask motor deficits.

814 Stroke not only causes brain injury but also impacts peripheral organs. Hypoxia and
815 vascular occlusion trigger the expression of adhesion molecules from endothelial cells, which,
816 along with BBB disruption, facilitate immune cell infiltration into the brain [4]. In line with this,
817 cortistatin restrained immune cell recruitment and activation, as shown by increased immune
818 infiltration in cortistatin-deficient mice, confirmed by both experimental and RNA-seq
819 deconvolution data. Our previous studies also demonstrated enhanced transmigration of
820 macrophages and T cells across cortistatin-deficient endothelium under inflammatory
821 conditions [14]. Moreover, cortistatin-deficient mice, regardless of age, displayed a heightened
822 pro-inflammatory cytokine profile alongside diminished anti-inflammatory signalling, features
823 generally correlated with increased infarct volume and poorer functional outcomes [55]. In
824 parallel, stroke triggers a systemic immunocompromised state, characterized by lymphoid
825 organ atrophy and infection susceptibility [56], likely mediated by neurohumoral pathways,
826 including glucocorticoid release, which can suppress adaptive immunity and exacerbate CNS
827 inflammation [57]. Consistently, cortistatin-deficient mice showed reduced spleen size and
828 cellularity, features strongly associated with poor stroke prognosis [58].

829 Beyond its role in peripheral immunity, we demonstrated that cortistatin critically
830 modulates neuroinflammation post-stroke, as shown by the increased number of immune-
831 related molecular terms in cortistatin-deficient brains. Microglia, the CNS primary immune
832 responders, rapidly accumulate in the peri-infarct and infarct areas following stroke [59]. While
833 young mice of both genotypes showed similar microglial/myeloid infiltration, it drastically
834 increased in the core of middle-aged cortistatin-deficient mice. In line with our previous studies
835 demonstrating exacerbated inflammatory responses from cortistatin-deficient microglia [9],
836 young cortistatin-deficient mice showed a more reactive microglial phenotype with reduced
837 anti-inflammatory markers (*i.e.,* CD163 and IL-10), indicating amplified neuroinflammatory
838 response [60,61]. Moreover, reactive microglia adopted hyper-ramified morphologies in

839 middle-aged *Cort*$^{-/-}$ mice, a phenotype related to excitotoxicity [39,46], harmful synaptic
840 pruning, and neuronal loss [62]. Similarly, Hinwood and colleagues reported that chronic
841 stress induces hyper-ramified microglia in rat prefrontal cortex, correlating with enhanced
842 neuronal activation and impaired spatial memory [63]. Accordingly, the stress-like behaviour
843 in these animals may indicate a pre-existing neuroinflammatory state that exacerbates
844 ischemic pathology.

845 Besides microglia, astrocytes critically contribute to neuroinflammation and glial scar
846 formation, which helps limit lesion spread and preserve viable neural tissue [64]. While
847 beneficial acutely, excessive or prolonged scarring may hinder regeneration and worsen long-
848 term outcomes [50]. Although not fully understood, the underlying molecular and cellular
849 mechanisms likely involve a complex balance of signals that can simultaneously boost
850 phagocytosis and debris clearance, essential for protecting the still-healthy tissue [64–66].
851 Importantly, impaired glial scar formation was observed in cortistatin-deficient mice following
852 acute stroke, particularly in middle-aged animals. Accordingly, defective astrocyte scar
853 formation in ischemia loss-of-function models leads to increased lesion size and
854 demyelination, resulting in impaired functional recovery [65–68]. However, in other
855 neuroinflammatory models, cortistatin-deficient astrocytes exhibited exacerbated reactivity at
856 chronic stages [9,13], when astrocyte responses can become chronic and detrimental. In this
857 sense, the impaired glial scar observed at the acute phase shifted to an exacerbated scarring
858 response during the subacute phase. These findings highlight the dynamic, stage-dependent
859 nature of astrocyte responses and suggest that cortistatin is essential for its temporal
860 regulation in ischemia. Furthermore, astrocytes in cortistatin-deficient mice displayed an
861 atypical phenotype, characterized by small, non-ramified, elongated morphologies not
862 previously described and worth further investigation. These atypical features were consistent
863 at both ages, indicating that cortistatin deficiency, followed by stroke, may accelerate age-
864 related outcomes. Indeed, recent findings demonstrate that in aged brains, stroke induces pro-
865 inflammatory astrocytes that may accelerate injury [43].

866 Aligned with morphological studies, deconvolution analysis confirmed a markedly
867 perturbed glial landscape in cortistatin-deficient mice, with increased signatures of both
868 activated and deactivated microglia and a shift in astrocytic phenotype. The loss of
869 homeostatic, neuroprotective astrocytes and the emergence of reactive, potentially neurotoxic
870 profiles imply a transition toward a maladaptive astroglial environment. This may compromise
871 metabolic support, glutamate clearance, and BBB integrity [50], worsening post-ischemic
872 dysfunction. Additionally, transcriptional evidence of impaired oligodendrocyte maturation and
873 myelination suggests that cortistatin deficiency may impede white matter recovery, potentially
874 affecting long-term cognitive and motor recovery [69].

875 On the other hand, BBB disruption is a key pathological hallmark of stroke, emerging
876 rapidly after artery occlusion and evolving through multiple phases, persisting for days to
877 weeks [70]. The significant increase in IgG extravasation in young and middle-aged cortistatin-
878 deficient mice after acute stroke supports our previous findings of heightened BBB
879 permeability in these mice under mild lipopolysaccharide-induced neuroinflammation [14].
880 Furthermore, BECs isolated from cortistatin-deficient mice displayed intrinsic endothelial
881 dysfunction at baseline, markedly exacerbated after ischemic injury (*i.e.,* increased
882 permeability, disruption of TJs, and a heightened pro-inflammatory state) [14]. Interestingly,
883 reduced cortistatin levels in BECs from both mice and humans were observed following
884 oxygen-glucose deprivation [14]. Furthermore, middle-aged cortistatin-deficient mice
885 exhibited reduced vascular density compared to their younger counterparts, a difference
886 absent in wild-type mice. Given age-related cerebrovascular decline [71], early vascular
887 deficits and BBB disruption in cortistatin-deficient mice highlight the essential role of cortistatin
888 in preserving cerebrovascular integrity. Moreover, our results provide the first evidence that
889 cortistatin deficiency accelerates age-associated cerebrovascular and neuroinflammatory
890 dysfunction. MCAO young cortistatin-deficient mice recapitulated several features typical of
891 aged wild-type animals, showing similar molecular signatures (*e.g.,* increased inflammation,
892 interferon signalling, and disrupted axonal and synaptic maintenance) [43], as well as

893 pathological manifestations including exacerbated microglial activation, astrocytic reactivity,
894 BBB disruption, and immune infiltration, underscoring the synergistic effects of cortistatin loss
895 and aging. While rodent aging models commonly involved animals aged 15–24 months
896 [72,73], the increased vulnerability and mortality risk of cortistatin-deficient mice under various
897 injury paradigms (including this study) [9,12,74–76], necessitate caution when working with
898 older cohorts.

899 According to our data of reduced cortistatin levels in human and mice during acute and
900 subacute stages, recent studies report a reduction of cortistatin expression in the ischemic
901 core, followed by a prolonged bilateral decrease, not seen with related neuropeptides like
902 somatostatin and ghrelin [44,77]. Conversely, somatostatin and neuropeptide Y-expressing
903 interneurons (which also secrete cortistatin) are selectively preserved in ischemia models
904 [78,79]. Remarkably, unlike somatostatin, which primarily affects inhibitory interneurons,
905 cortistatin exhibits broader immunomodulatory and vasoregulatory functions [14,80],
906 supporting its unique role in stroke pathology. Reduced cortistatin expression is also linked to
907 other neurodegenerative/neurovascular disorders, including Alzheimer's disease [81] and
908 diabetic retinopathy [82]. Moreover, deletion of the chromosomal region 1p36, containing the
909 cortistatin gene, causes severe neurological and developmental deficits in humans [83]. These
910 findings collectively underscore the critical role of maintaining physiological cortistatin levels
911 to preserve neurovascular homeostasis and mitigate neuroinflammatory damage. Future
912 research should explore whether cortistatin expression dynamics may serve as a prognostic
913 biomarker for stroke or other neuroimmune disorders.

914 Considering the narrow therapeutic window of current interventions like rtPA (4-6h) and
915 endovascular thrombectomy (up to 24h), investigating endogenous mechanisms and
916 therapeutic interventions within the first 48h is essential, as it can determine long-term
917 outcome [2]. Our data demonstrate an early dysregulation in cortistatin-deficient mice during
918 acute stroke characterized by insufficient activation or downregulation of terms related to
919 inflammation resolution, tissue repair, neurogenesis, synaptic plasticity, and cognition.

920 Importantly, this appears to impair the subsequent recovery process, as by 7 days post-injury,
921 these mice exhibited reduced neuronal repopulation, impaired axonal integrity, aberrant glial
922 scar formation, and decreased VEGF expression, all key processes involved in recovery and
923 neurogenesis. VEGF supports neurovascular remodelling, neuroprotection, and progenitor
924 cell proliferation [83]. Myelin regeneration is also crucial for recovery, as oligodendrocyte death
925 and persistent demyelination contribute to long-term deficits [69]. Notably, cortistatin-deficient
926 mice show abnormal myelin in multiple sclerosis models [42], suggesting a role for cortistatin
927 in axonal integrity and neurorepair, though mechanisms remain unclear.

928 Consistent cortistatin downregulation in human stroke and its causal role in
929 exacerbating post-ischemic pathology in animal models suggest that restoring cortistatin could
930 represent a novel therapeutic strategy. Acute administration reduced neurological score and
931 lesion size in cortistatin-deficient mice, similar to levels observed in wild-type young mice. In
932 young animals, this neuroprotective effect was linked to increased BDNF and GDNF
933 expression, known to support neurogenesis and recovery [84,85]. Beyond neuronal
934 protection, cortistatin treatment modulated systemic immune responses, normalized microglial
935 phenotypes, and restored astrocytic responses to wild-type levels. Cortistatin may influence
936 immune modulation through multiple avenues, including direct effects on immune cells, as
937 evidenced by its *in vitro* immunosuppressive effects on activated macrophages [86], as well
938 as through maintaining endothelial barrier integrity. While some studies indicate that
939 suppressing immune activation may increase infection susceptibility due to post-stroke
940 immunosuppression, complicating the risk-benefit profile of anti-inflammatory therapies [57],
941 our findings demonstrate that cortistatin exerts a context-dependent modulation of glial and
942 immune responses. This aligns with the emerging consensus that therapeutic strategies must
943 be temporally and contextually tailored [15,87]. Moreover, its administration reduced BBB
944 leakage in young and middle-aged animals, highlighting its potential as a therapeutic agent in
945 mitigating BBB breakdown. Strikingly, cortistatin treatment reversed most pathological

946 features at the subacute stage, indicating that its neuroprotective effects extend beyond the
947 acute phase and promote sustained recovery.

948 Importantly, the ability of cortistatin to improve outcomes in middle-aged or highly
949 susceptible mice suggests a robust pleiotropic mechanism that can overcome documented
950 failure of neuroimmune-targeted therapies in aged patients. However, while cortistatin
951 treatment improved neurological scores, it did not significantly affect motor coordination in
952 middle-aged mice, unlike in younger ones, possibly due to age-related apathetic behavior
953 linked to the role of cortistatin in locomotor activity [5]. Critical questions remain about its role
954 in motivational and locomotor circuits, possibly tied to interactions with the dopaminergic
955 system (significantly affected when cortistatin is absent, as described here), which warrant
956 further investigation.

957 In conclusion, the present study advances our understanding of stroke pathophysiology
958 by identifying cortistatin as a pivotal neuroimmune regulator, whose loss or decrease
959 exacerbates brain injury by affecting central and peripheral immune responses, neurovascular
960 integrity, and glial function. These findings support the emerging consensus that stroke is not
961 a localized cerebrovascular insult but rather a complex, multi-organ syndrome involving
962 dysregulated systemic and neuroimmune communication [2,88]. Our data demonstrate that
963 cortistatin, traditionally studied for its roles in sleep, stress, and immune modulation, protects
964 throughout multiple stages of ischemic injury, from acute damage (glial reactivity or BBB
965 breakdown) to tissue repair and neurovascular remodeling. Moreover, cortistatin is crucial for
966 balancing the neuroimmune axis, mitigating excessive inflammation both centrally and
967 peripherally, and promoting glial homeostasis and repair, counteracting the effects of chronic
968 stress and aging. Additionally, the lack of cortistatin accelerates aging-like neuroimmune and
969 vascular decline, highlighting its critical role in maintaining cerebrovascular health. Without
970 cortistatin, impaired neurorepair, neuroinflammation, and BBB dysfunction hinder stroke
971 recovery. From the therapeutic perspective, the fact that exogenous cortistatin administration
972 reverses many pathological features and improves outcomes in both young and middle-aged

973 mice is particularly noteworthy. This supports that targeting endogenous neuroimmune
974 modulators could extend the therapeutic window and provide benefit beyond current time-
975 limited interventions. Altogether, our findings provide critical insights into the stroke
976 pathophysiology and pave the way for novel therapeutic approaches targeting neurovascular
977 dysfunction, glial overactivation, and maladaptive neuroimmune responses. Finally, the
978 translational relevance is strengthened by human transcriptomic data showing consistently
979 reduced cortistatin levels across multiple datasets, tissues, and disease stages, highlighting
980 its potential as a biomarker for stroke severity and progression.

981 **ACKNOWLEDGEMENTS**

982 The authors would like to thank the Animal Care Unit and Microscopy Service Unit staff from
983 the IPBLN for their technical support.

984 **FUNDING**

985 This work was supported by the Spanish Ministry of Economy and Competitiveness
986 (MCIN)/Spanish Research Agency (AEI)/10.13039/501100011033 grants: SAF2017-85602-R
987 and PID2020-119638RB-I00 (to E.G-R.), FPU-program FPU17/02616 and Ramón Areces
988 Foundation post-doctoral fellowship (to J.C-G.), FPI-program PRE2018-084824 (to I.S-M.)
989 and PRE2021-100172 (to P.V-R.); the grant PROYEXCEL_00867 from the Regional
990 Andalusian Government (to E.G.-R.); the Swiss Science Foundation FNS 310030_212233
991 grant to L.H

992 **CONTRIBUTIONS**

993 E.G-R conceived, designed, and supervised the entire study. J.C-G and E.G-R outlined the
994 experiments and analysed all the data. J.C-G, P.V-R, I.S-M, A.C-M, and I.F-L performed the
995 experiments. P.V-R and JL. R analysed and interpreted the transcriptomic data. J.C-G, L.B,
996 M.P, L.H, and E.G-R contributed to data interpretation and discussion of the results. J.C-G
997 and E.G-R wrote and revised the manuscript. All authors have read and approved the final
998 version of the manuscript.

BIBLIOGRAPHY

1. Campbell BCV, De Silva DA, Macleod MR, Coutts SB, Schwamm LH, Davis SM, et al. Ischaemic stroke. Nat Rev Dis Primers. 2019;5:1–22.
2. Iadecola C, Anrather J. The immunology of stroke: from mechanisms to translation. Nat Med. 2011;17:796–808.
3. Drieu A, Levard D, Vivien D, Rubio M. Anti-inflammatory treatments for stroke: from bench to bedside. Ther Adv Neurol Disord. 2018;11:1756286418789854.
4. Anrather J, Iadecola C. Inflammation and Stroke: An Overview. Neurotherapeutics. 2016;13:661–70.
5. de Lecea L, Criado JR, Prospero-Garcia O, Gautvik KM, Schweitzer P, Danielson PE, et al. A cortical neuropeptide with neuronal depressant and sleep-modulating properties. Nature. 1996;381:242–5.
6. Delgado M, Gonzalez-Rey E. Role of Cortistatin in the Stressed Immune System. In: Savino W, Guaraldi F, editors. Frontiers of Hormone Research. S. Karger AG; 2017. p. 110–20.
7. Córdoba-Chacón J, Gahete MD, Pozo-Salas AI, Martínez-Fuentes AJ, de Lecea L, Gracia-Navarro F, et al. Cortistatin is not a somatostatin analogue but stimulates prolactin release and inhibits GH and ACTH in a gender-dependent fashion: potential role of ghrelin. Endocrinology. 2011;152:4800–12.
8. Deghenghi R, Papotti M, Ghigo E, Muccioli G. Cortistatin, but not somatostatin, binds to growth hormone secretagogue (GHS) receptors of human pituitary gland. J Endocrinol Invest. 2001;24:RC1-3.
9. Souza-Moreira L, Morell M, Delgado-Maroto V, Pedreño M, Martinez-Escudero L, Caro M, et al. Paradoxical Effect of Cortistatin Treatment and Its Deficiency on Experimental Autoimmune Encephalomyelitis. J Immunol. 2013;191:2144–54.
10. Braun H, Schulz S, Becker A, Schröder H, Höllt V. Protective effects of cortistatin (CST-14) against kainate-induced neurotoxicity in rat brain. Brain Res. 1998;803:54–60.
11. Chiu C-T, Wen L-L, Pao H-P, Wang J-Y. Cortistatin Is Induced in Brain Tissue and Exerts Neuroprotection in a Rat Model of Bacterial Meningoencephalitis. J Infect Dis. 2011;204:1563–72.
12. Falo CP, Benitez R, Caro M, Morell M, Forte-Lago I, Hernandez-Cortes P, et al. The Neuropeptide Cortistatin Alleviates Neuropathic Pain in Experimental Models of Peripheral Nerve Injury. Pharmaceutics. 2021;13:947.
13. Serrano-Martínez I, Pedreño M, Castillo-González J, Ferraz-de-Paula V, Vargas-Rodríguez P, Forte-Lago I, et al. Cortistatin as a Novel Multimodal Therapy for the Treatment of Parkinson's Disease. Int J Mol Sci. 2024;25:694.
14. Castillo-González J, Ruiz JL, Serrano-Martínez I, Forte-Lago I, Ubago-Rodriguez A, Caro M, et al. Cortistatin deficiency reveals a dysfunctional brain endothelium with impaired gene pathways, exacerbated immune activation, and disrupted barrier integrity. J Neuroinflammation. 2023;20:226.
15. Castillo-González J, Buscemi L, Vargas-Rodríguez P, Serrano-Martínez I, Forte-Lago I, Caro M, et al. Cortistatin exerts an immunomodulatory and neuroprotective role in a preclinical model of ischemic stroke. Pharmacol Res. 2024;210:107501.
16. Barriga M, Benitez R, Robledo G, Caro M, O'Valle F, Campos-Salinas J, et al. Neuropeptide Cortistatin Regulates Dermal and Pulmonary Fibrosis in an Experimental Model of Systemic Sclerosis. Neuroendocrinology. 2021;112:784–95.
17. Buscemi L, Price M, Bezzi P, Hirt L. Spatio-temporal overview of neuroinflammation in an experimental mouse stroke model. Sci Rep. 2019;9:507.
18. Lee H. Disruption of the blood-brain barrier in parkinson's disease: curse or route to a cure? Front Biosci. 2014;19:272.
19. Buscemi L, Price M, Castillo-González J, Chatton J-Y, Hirt L. Lactate Neuroprotection against Transient Ischemic Brain Injury in Mice Appears Independent of HCAR1 Activation. Metabolites. 2022;12:465.
20. Huang S, Ren C, Luo Y, Ding Y, Ji X, Li S. New insights into the roles of oligodendrocytes regulation in ischemic stroke recovery. Neurobiol Dis. 2023;184:106200.
21. Zhang Q, Heng Y, Mou Z, Huang J, Yuan Y, Chen N. Reassessment of subacute MPTP-treated mice as animal model of Parkinson's disease. Acta Pharmacol Sin. 2017;38:1317–28.
22. Young K, Morrison H. Quantifying Microglia Morphology from Photomicrographs of Immunohistochemistry Prepared Tissue Using ImageJ. JoVE. 2018;57648.

23. Fernández-Arjona M del M, Grondona JM, Granados-Durán P, Fernández-Llebrez P, López-Ávalos MD. Microglia Morphological Categorization in a Rat Model of Neuroinflammation by Hierarchical Cluster and Principal Components Analysis. Front Cell Neurosci. 2017;11:235.
24. Schindelin J, Arganda-Carreras I, Frise E, Kaynig V, Longair M, Pietzsch T, et al. Fiji: an open-source platform for biological-image analysis. Nat Methods. 2012;9:676–82.
25. Ruiz JL, Terrón-Camero LC, Castillo-González J, Fernández-Rengel I, Delgado M, Gonzalez-Rey E, et al. reanalyzerGSE: tackling the everlasting lack of reproducibility and reanalyses in transcriptomics. bioRxiv; 2023.
26. Ashburner M, Ball CA, Blake JA, Botstein D, Butler H, Cherry JM, et al. Gene Ontology: tool for the unification of biology. Nat Genet. 2000;25:25–9.
27. The Gene Ontology Consortium. The Gene Ontology resource: enriching a GOld mine. Nucleic Acids Res. 2021;49:D325–34.
28. Mancarci BO, Toker L, Tripathy SJ, Li B, Rocco B, Sibille E, et al. Cross-Laboratory Analysis of Brain Cell Type Transcriptomes with Applications to Interpretation of Bulk Tissue Data. eNeuro. 2017;4:ENEURO.0212-17.2017.
29. Zheng K, Lin L, Jiang W, Chen L, Zhang X, Zhang Q, et al. Single-cell RNA-seq reveals the transcriptional landscape in ischemic stroke. J Cereb Blood Flow Metab. 2022;42:56–73.
30. Zhu W, Tian L, Yue X, Liu J, Fu Y, Yan Y. LncRNA Expression Profiling of Ischemic Stroke During the Transition From the Acute to Subacute Stage. Front Neurol. 2019;10:36.
31. Han R, Zhang P, Li H, Chen Y, Hao Y, Guo Q, et al. Differential Expression and Correlation Analysis of Global Transcriptome for Hemorrhagic Transformation After Acute Ischemic Stroke. Front Neurosci. 2022;16.
32. Kanki H, Matsumoto H, Togami Y, Okuzaki D, Ogura H, Sasaki T, et al. Importance of microRNAs by mRNA-microRNA integration analysis in acute ischemic stroke patients. J Stroke Cerebrovasc Dis. 2023;32:107277.
33. Huttner HB, Bergmann O, Salehpour M, Rácz A, Tatarishvili J, Lindgren E, et al. The age and genomic integrity of neurons after cortical stroke in humans. Nat Neurosci. 2014;17:801–3.
34. Huang X, Guo M, Zhang Y, Xie J, Huang R, Zuo Z, et al. Microglial IL-1RA ameliorates brain injury after ischemic stroke by inhibiting astrocytic CXCL1-mediated neutrophil recruitment and microvessel occlusion. Glia. 2023;71:1607–25.
35. Wang Y, Bai Y, Cai Y, Zhang Y, Shen L, Xi W, et al. Circular RNA SCMH1 suppresses KMO expression to inhibit mitophagy and promote functional recovery following stroke. Theranostics. 2024;14:7292–308.
36. Stokowska A, Aswendt M, Zucha D, Lohmann S, Wieters F, Suarez JM, et al. Complement C3a treatment accelerates recovery after stroke via modulation of astrocyte reactivity and cortical connectivity. J Clin Invest. 2023;133.
37. Wang J, Zhang P, Tang Z. Animal models of transient ischemic attack: a review. Acta Neurol Belg. 2020;120:267–75.
38. Katchanov J, Waeber C, Gertz K, Gietz A, Winter B, Brück W, et al. Selective neuronal vulnerability following mild focal brain ischemia in the mouse. Brain Pathol. 2003;13:452–64.
39. Choi YH, Laaker C, Hsu M, Cismaru P, Sandor M, Fabry Z. Molecular Mechanisms of Neuroimmune Crosstalk in the Pathogenesis of Stroke. Int J Mol Sci. 2021;22:9486.
40. Fisher M, Feuerstein G, Howells DW, Hurn PD, Kent TA, Savitz SI, et al. Update of the stroke therapy academic industry roundtable preclinical recommendations. Stroke. 2009;40:2244–50.
41. Savitz SI, Baron J-C, Fisher M, STAIR X Consortium. Stroke Treatment Academic Industry Roundtable X: Brain Cytoprotection Therapies in the Reperfusion Era. Stroke. 2019;50:1026–31.
42. Pérez Falo C. Papel del neuropéptido cortistatina en la fisiopatología de los procesos de des- y remielinización en el sistema nervioso [Internet]. Universidad de Granada; 2021. Available from: https://dialnet.unirioja.es/servlet/tesis?codigo=295627
43. Androvic P, Kirdajova D, Tureckova J, Zucha D, Rohlova E, Abaffy P, et al. Decoding the Transcriptional Response to Ischemic Stroke in Young and Aged Mouse Brain. Cell Rep. 2020;31:107777.
44. Han B, Zhou S, Zhang Y, Chen S, Xi W, Liu C, et al. Integrating spatial and single-cell transcriptomics to characterize the molecular and cellular architecture of the ischemic mouse brain. Sci Transl Med. 2024;16:eadg1323.
45. Stuckey SM, Ong LK, Collins-Praino LE, Turner RJ. Neuroinflammation as a Key Driver of Secondary Neurodegeneration Following Stroke? Int J Mol Sci. 2021;22:13101.

46. Vidal-Itriago A, Radford RAW, Aramideh JA, Maurel C, Scherer NM, Don EK, et al. Microglia morphophysiological diversity and its implications for the CNS. Front Immunol. 2022;13.
47. Herpich F, Rincon F. Management of Acute Ischemic Stroke. Crit Care Med. 2020;48:1654.
48. Cai W, Liu H, Zhao J, Chen LY, Chen J, Lu Z, et al. Pericytes in Brain Injury and Repair After Ischemic Stroke. Transl Stroke Res. 2017;8:107–21.
49. Qin C, Zhou L-Q, Ma X-T, Hu Z-W, Yang S, Chen M, et al. Dual Functions of Microglia in Ischemic Stroke. Neurosci Bull. 2019;35:921–33.
50. Li L, Zhou J, Han L, Wu X, Shi Y, Cui W, et al. The Specific Role of Reactive Astrocytes in Stroke. Front Cell Neurosci. 2022;16.
51. Ardelt AA, Anjum N, Rajneesh KF, Kulesza P, Koehler RC. Estradiol augments peri-infarct cerebral vascular density in experimental stroke. Experiment Neurol. 2007;206:95–100.
52. Fan C, Zhang L, He Z, Shao P, Ding L, Wang G, et al. Reduced Severity of Outcome of Recurrent Ipsilateral Transient Cerebral Ischemia Compared with Contralateral Transient Cerebral Ischemia in Rats. J Stroke Cerebrovasc Dis. 2017;26:2915–25.
53. Pinto R, Magalhães A, Sousa M, Melo L, Lobo A, Barros P, et al. Bridging the Transient Intraluminal Stroke Preclinical Model to Clinical Practice: From Improved Surgical Procedures to a Workflow of Functional Tests. Front Neurol. 2022;13.
54. Benakis C, Garcia-Bonilla L, Iadecola C, Anrather J. The role of microglia and myeloid immune cells in acute cerebral ischemia. Front Cell Neurosci. 2015;8.
55. Doll DN, Barr TL, Simpkins JW. Cytokines: Their Role in Stroke and Potential Use as Biomarkers and Therapeutic Targets. Aging Dis. 2014;5:294–306.
56. Westendorp WF, Dames C, Nederkoorn PJ, Meisel A. Immunodepression, Infections, and Functional Outcome in Ischemic Stroke. Stroke. 2022;53:1438–48.
57. Iadecola C, Buckwalter MS, Anrather J. Immune responses to stroke: mechanisms, modulation, and therapeutic potential. J Clin Invest. 2020;130:2777–88.
58. Faura J, Bustamante A, Miró-Mur F, Montaner J. Stroke-induced immunosuppression: implications for the prevention and prediction of post-stroke infections. J Neuroinflammation. 2021;18:127.
59. Peng L, Hu G, Yao Q, Wu J, He Z, Law BY-K, et al. Microglia autophagy in ischemic stroke: A double-edged sword. Front Immunol. 2022;13.
60. Xue Y, Nie D, Wang L-J, Qiu H-C, Ma L, Dong M-X, et al. Microglial Polarization: Novel Therapeutic Strategy against Ischemic Stroke. Aging Dis. 2021;12:466–79.
61. Laffer B, Bauer D, Wasmuth S, Busch M, Jalilvand TV, Thanos S, et al. Loss of IL-10 Promotes Differentiation of Microglia to a M1 Phenotype. Front Cell Neurosci. 2019;13.
62. Neher JJ, Emmrich JV, Fricker M, Mander PK, Théry C, Brown GC. Phagocytosis executes delayed neuronal death after focal brain ischemia. Proc Natl Acad Sci U S A. 2013;110:E4098–107.
63. Hinwood M, Morandini J, Day TA, Walker FR. Evidence that Microglia Mediate the Neurobiological Effects of Chronic Psychological Stress on the Medial Prefrontal Cortex. Cereb Cortex. 2012;22:1442–54.
64. Shen X-Y, Gao Z-K, Han Y, Yuan M, Guo Y-S, Bi X. Activation and Role of Astrocytes in Ischemic Stroke. Front Cell Neurosci. 2021;15.
65. Burda JE, Sofroniew MV. Reactive Gliosis and the Multicellular Response to CNS Damage and Disease. Neuron. 2014;81:229–48.
66. Wanner IB, Anderson MA, Song B, Levine J, Fernandez A, Gray-Thompson Z, et al. Glial Scar Borders Are Formed by Newly Proliferated, Elongated Astrocytes That Interact to Corral Inflammatory and Fibrotic Cells via STAT3-Dependent Mechanisms after Spinal Cord Injury. J Neurosci. 2013;33:12870–86.
67. Faulkner JR, Herrmann JE, Woo MJ, Tansey KE, Doan NB, Sofroniew MV. Reactive astrocytes protect tissue and preserve function after spinal cord injury. J Neurosci. 2004;24:2143–55.
68. Herrmann JE, Imura T, Song B, Qi J, Ao Y, Nguyen TK, et al. STAT3 is a critical regulator of astrogliosis and scar formation after spinal cord injury. J Neurosci. 2008;28:7231–43.
69. Cheng Y-J, Wang F, Feng J, Yu B, Wang B, Gao Q, et al. Prolonged myelin deficits contribute to neuron loss and functional impairments after ischaemic stroke. Brain. 2024;147:1294–311.
70. Bernardo-Castro S, Sousa JA, Brás A, Cecília C, Rodrigues B, Almendra L, et al. Pathophysiology of Blood–Brain Barrier Permeability Throughout the Different Stages of Ischemic Stroke and Its Implication on Hemorrhagic Transformation and Recovery. Front Neurol. 2020;11.

71. Yousufuddin M, Young N. Aging and ischemic stroke. Aging (Albany NY). 2019;11:2542–4.
72. Ritzel RM, Lai Y-J, Crapser JD, Patel AR, Schrecengost A, Grenier JM, et al. Aging alters the immunological response to ischemic stroke. Acta Neuropathol. 2018;136:89–110.
73. Sieber MW, Claus RA, Witte OW, Frahm C. Attenuated Inflammatory Response in Aged Mice Brains following Stroke. PLoS One. 2011;6:e26288.
74. Morell M, Souza-Moreira L, Caro M, O'Valle F, Forte-Lago I, de Lecea L, et al. Analgesic effect of the neuropeptide cortistatin in murine models of arthritic inflammatory pain. Arthritis Rheum. 2013;65:1390–401.
75. Barriga M, Benitez R, Ferraz-de-Paula V, Garcia-Frutos M, Caro M, Robledo G, et al. Protective role of cortistatin in pulmonary inflammation and fibrosis. Br J Pharmacol. 2021;178:4368–88.
76. Benitez R, Caro M, Andres-Leon E, O'Valle F, Delgado M. Cortistatin regulates fibrosis and myofibroblast activation in experimental hepatotoxic- and cholestatic-induced liver injury. Br J Pharmacol. 2022;179:2275–96.
77. Rauca C, Schäfer K, Höllt V. Effects of somatostatin, octreotide and cortistatin on ischaemic neuronal damage following permanent middle cerebral artery occlusion in the rat. Naunyn-Schmiedeberg's Arch Pharmacol. 1999;360:633–8.
78. Uemura Y, Kowall NW, Beal MF. Selective sparing of NADPH-diaphorase-somatostatin-neuropeptide Y neurons in ischemic gerbil striatum. Ann Neurol. 1990;27:620–5.
79. Larsson E, Lindvall O, Kokaia Z. Stereological assessment of vulnerability of immunocytochemically identified striatal and hippocampal neurons after global cerebral ischemia in rats. Brain Res. 2001;913:117–32.
80. Ferone D, Hagen PM van, Semino C, Dalm VA, Barreca A, Colao A, et al. Somatostatin receptor distribution and function in immune system. Dig Liver Dis. 2004;36:S68–77.
81. Gahete MD, Rubio A, Durán-Prado M, Avila J, Luque RM, Castaño JP. Expression of Somatostatin, cortistatin, and their receptors, as well as dopamine receptors, but not of neprilysin, are reduced in the temporal lobe of Alzheimer's disease patients. J Alzheimers Dis. 2010;20:465–75.
82. Carrasco E, Hernández C, de Torres I, Farrés J, Simó R. Lowered cortistatin expression is an early event in the human diabetic retina and is associated with apoptosis and glial activation. Mol Vis. 2008;14:1496–502.
83. Jordan VK, Zaveri HP, Scott DA. 1p36 deletion syndrome: an update. TACG. 2015;8:189–200.
84. Liu Y, Wang S, Luo S, Li Z, Liang F, Zhu Y, et al. Intravenous PEP-1-GDNF is protective after focal cerebral ischemia in rats. Neurosci Lett. 2016;617:150–5.
85. Schäbitz W-R, Steigleder T, Cooper-Kuhn CM, Schwab S, Sommer C, Schneider A, et al. Intravenous brain-derived neurotrophic factor enhances poststroke sensorimotor recovery and stimulates neurogenesis. Stroke. 2007;38:2165–72.
86. Gonzalez-Rey E, Chorny A, Robledo G, Delgado M. Cortistatin, a new antiinflammatory peptide with therapeutic effect on lethal endotoxemia. J Exp Med. 2006;203:563–71.
87. Krakauer JW. The complex dynamics of stroke onset and progression. Curr Opin Neurol. 2007;20:47–50.
88. Chamorro Á, Meisel A, Planas AM, Urra X, van de Beek D, Veltkamp R. The immunology of acute stroke. Nat Rev Neurol. 2012;8:401–10.